NOTICE

The quality of this microform is heavily dependent upon the quality of the original thesis submitted for microfilming. Every effort has been made to ensure the highest quality of reproduction possible.

If pages are missing, contact the university which granted the degree.

Some pages may have indistinct print especially if the original pages were typed with a poor typewriter ribbon or if the university sent us an inferior photocopy.

Reproduction in full or in part of this microform is governed by the Canadian Copyright Act, R.S.C. 1970, c. C-30, and subsequent amendments.

AVIS

La qualité de cette microforme dépend grandement de la qualité de la thèse soumise au microfilmage. Nous avons tout fait pour assurer une qualité supérieure de reproduction.

S'il manque des pages, veuillez communiquer avec l'université qui a conféré le grade.

La qualité d'impression de certaines pages peut laisser à désirer, surtout si les pages originales ont été dactylographiées à l'aide d'un ruban usé ou si l'université nous a fait parvenir une photocopie de qualité inférieure.

La reproduction, même partielle, de cette microforme est soumise à la Loi canadienne sur le droit d'auteur, SRC 1970, c. C-30, et ses amendements subséquents.

ISBN 0-315-59167-6

Photocurrent Generation and Charge Transport in Ion-Exchange Polymer Films Containing Zinc Meso-Tetraphenyl-Porphyrin

Zhiqing Huang

A Thesis

in

The Department

of

Physics

Presented in Partial Fulfillment of the Requirements
for the Degree of Master of Science at
Concordia University
Montreal, Quebec, Canada

April, 1990

Abstract

Photocurrent Generation and Charge Transport in Ion-Exchange Polymer Films Containing Zinc Meso-Tetraphenyl-Porphyrin

Zhiqing Huang

Various methods have been used to investigate the photocurrent generation and charge transport in the system composed of zinc meso- tetraphenyl-porphyrin (ZnTPP) dye molecules incorporated in an ion-exchange polymer blend on SnO_2 optically transparent electrodes(OTE).

The dark conductivity measurements performed on these films with or without the dye in solid phase show that the trap present is associated with the polymer and is not significantly influenced by the presence of the dye. The results also show that these ion-exchange polymer blend films with or without the dye behave, to a certain degree, similarly to doped or undoped conventional semiconductors.

Photoconductivity measurements performed on these dye-loaded ion-exchange polymer blend films show that these cells are capable of photoinduced charge separation when illuminated with the wavelengths absorbed by the dye. The results obtained indicate that electrons may be transferred from the photoexcited dyes to the polymer matrix and transported to the SnO_2 substrate.

Charge transport in these solid-state cells is believed to proceed via electronic conduction mechanisms which are

intimately related to the internal morphology of the ZnTPP/polyXIO films. The model is essentially based upon the energetic relation between the individual components of the system and invokes the distribution of donor and acceptor states associated with the hydrophobic domains of the polymer blend to explain the photoinduced charge migration.

Acknowledgements

I wish to thank the people who helped me in this endeavor:

Dr. Marcus F.Lawrence for his patient guidance throughout this interdisciplinary program. His dedication to research and teaching will always be an inspiration to me;

Prof. B. Frank and Prof. Sushil K. Misra for their kind assistance in my course work;

Dr. Ishmael D. Ordoñez and Dr. David A. Biro for their useful discussions on polymer casting techniques;

Mr. Mark Lefebvre and Dr. Ishmael D. Ordoñez who supplied me with the random quaternary copolymer solution used in this work.

Mrs. Gloria Thompson for her administrative and technical support;

Both the Department of Physics and Department of Chemistry which make this interdisciplinary program possible;

My wife, Xinheng, for her love and support, and lovely daughter, Nuoxin

To my Family

Table of Contents

List of Figures

List of Tables

List of Symbols

a, a_1, a_2	Constants in solution of rate equations
C_{nt}	Transition probability
ε_o	Permittivity of free space
E_c	Lowest energy of the conduction band
E_g	Band gap
E_v	highest energy of the valence band
e_{nt}	Transition probability
$f(E)$	State occupation probability
I	Current
I_o	Dark current
I_{ph}	Photocurrent
k	Boltzmann's constant
L	Length of specimen
μ	Drift mobility
μ_o	microscopic mobility
N_t	Density of traps
n	Density of free electrons
n_o	Steady-state density of free electrons
σ	Conductivity
σ_o	preexponential conductivity
ρ	Specific resistivity
$\rho_A(E)$, $\rho_D(E)$	Densities of molecular ion acceptor states, and donor states, respectively

t	Time
ϕ	Fraction of free to trapped carriers
τ	Lifetime
τ_1, τ_2	Response times
V	Applied voltage

CHAPTER 1

INTRODUCTION

1.1 OVERVIEW

It is not many years ago when the interest in the electrical properties of polymers was effectively limited to their electrical insulating ability. However this situation has changed remarkably in recent years and it is likely that the future will show an even greater expansion of interest into electrical properties of polymeric materials. The reason is basically two fold, firstly, electrical measurements give an excellent diagnostic approach, in that they reflect macromolecular electrical structure and motion, both in solution and the solid state. Secondly is the potential technical application of their electrical properties.

Of particular interest here are recent developments concerning the use of ion-exchange polymers to produce electrodes with surfaces that have a high affinity for redox reactants[1-13]. This polymer is a blend which consists of a random quaternary copolymer containing two types of hydrophilic cationic groups and one hydrophobic styrene

group, as depicted in Figure 1.1A, mixed with poly[(4-vinylpyridine) -*co*-styrene](PVP), depicted in Figure 1.1B. Studies made with this polymer have led to interesting results with respect to the fabrication of synthetic organic/inorganic systems capable of photoinduced charge separation. The main feature of this type of polymer is its spontaneous tendency to segregate into hydrophilic and hydrophobic domains following casting of films from methanol solution(solvent evaporation) onto substrates. The photoelectric behavior of SnO_2 coated with ion-exchange polymers to which soluble dye molecules(porphyrins, phthalocyanines) or CdS particles have been added, has been studied under electrochemical(hexacyanoferrate [II,III] electrolyte, Pt counter-electrode) conditions. Upon illumination of these systems, photocurrent can be generated through light absorption by either the organic or the inorganic photoactive species involved, and charge transport was assumed to proceed via both "dry" electronic and ionic conduction mechanisms through the polymer.

Following these observation a model based essentially upon the energetic relation between the individual components of the system, and which invokes the distributions of donor and acceptor states associated with the polymer, was proposed to account for the vectorial migration of photogenerated charges[14]. Even though the conversion efficiency for this type of system is quite low at the moment, it remains of

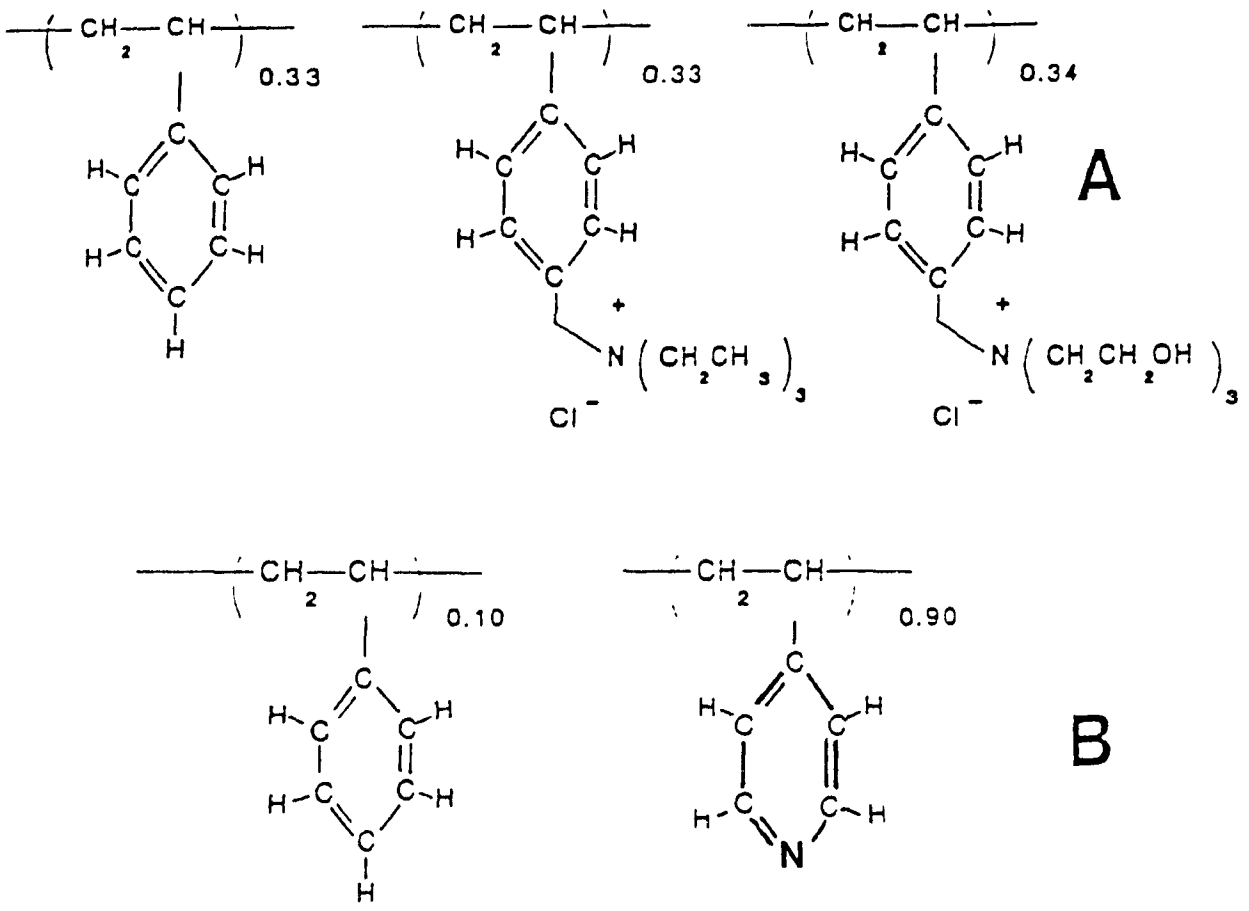

FIGURE 1.1 Structure of polymers used in the ion-exchange polymer blend: **A.** random quaternary copolymer and **B.** poly [(4-vinylpyridine)-*co*-styrene](PVP)

interest because of the important role it can play in providing a robust support for immobilizing photo- or electro-active species at a solid/solid or solid/electrolyte interface.

In this thesis, to better characterize the dry electronic transport of photogenerated charges to the SnO_2 electrode through the polymer film, we deal with the molecular doping of one such ion-exchange polymer in the solid-state. The dark conductive and photoconductive behavior of SnO_2 optically transparent electrodes (OTE), coated with the ion-exchange polymer(Figure 1.1) in which soluble dye molecules have been incorporated (ZnTPP), is described.

It was found that the dye/polymer system's photo-current-time responses are parallel to those obtained for the wet (photoelectrochemical) cells previously studied [14-16]. The time constants for dry and wet cells are not experimentally distinguishable which implies that the time constants refer to charge-transport processes in the solid phase[16]. This is a synthetic organic system which is, therefore, capable of spatial separation of photogenerated charges (electron-hole pairs). A simple version of this process is shown in the scheme(next page), which illustrates that by irradiating a dye molecule in the presence of appropriate donors and acceptors, one may expect vectorial charge migration. An excited electron can be transferred from the dye to acceptor A_1, leaving a positive hole behind.

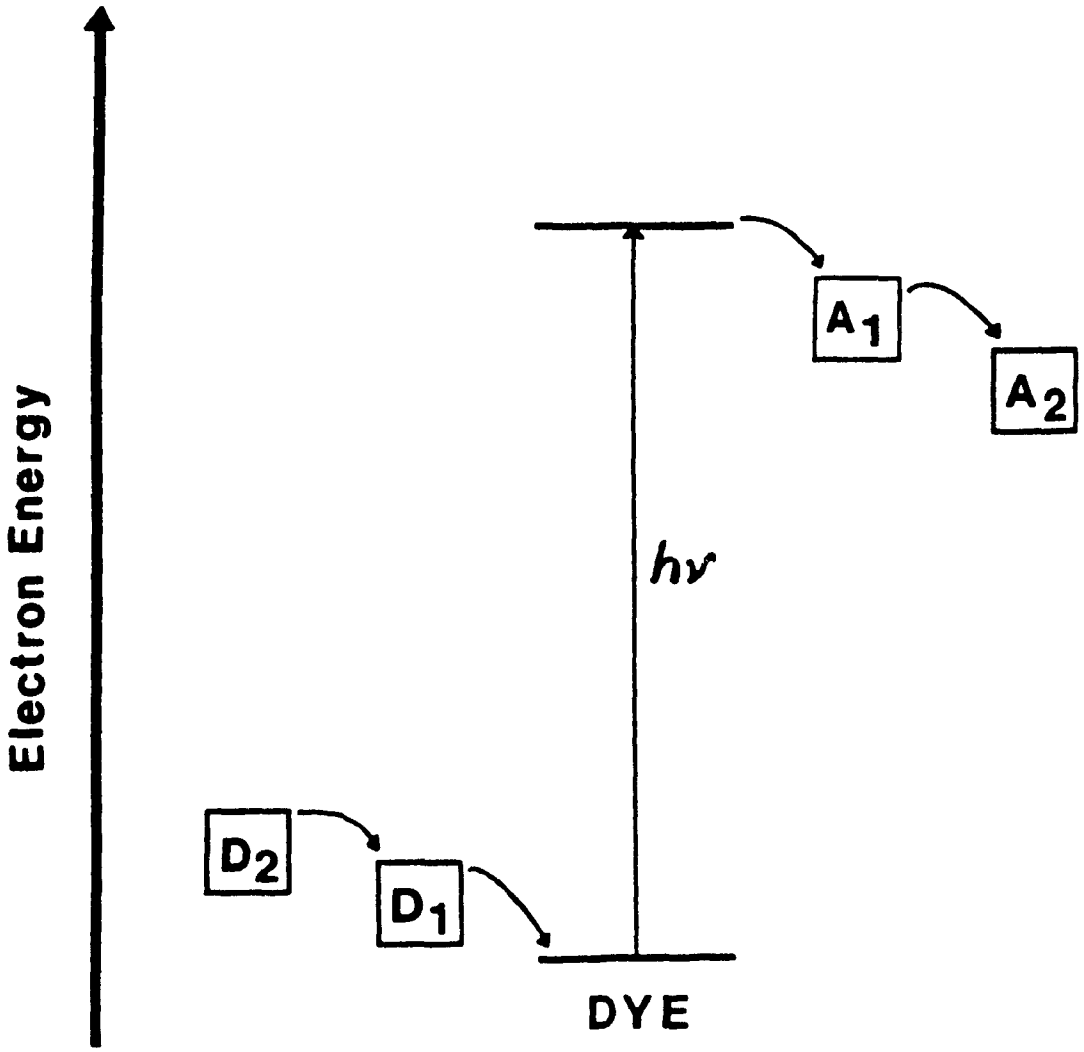

FIGURE 1.2 A simple version of spatial separation of photogenerated charges

This positive hole can be reduced by an electron from donor D_1. The overall result is the migration of an electron and a hole in opposite directions, and, therefore, electrical current. An overview of the fundamental concepts and materials used in this study constitutes the remaining sections of this chapter. Some of the theoretical aspects will be treated more specifically in subsequent chapters.

1.2 INTRODUCTORY DEFINITIONS AND CONCEPTS

1.2.1 POLYMERS

Despite the variety of polymeric materials available certain principles apply to all polymers. They are materials of high molecular weight formed by linking a large number of simple chemical units (the monomers). The structural units can be linked together in a variety of ways depending upon their chemistry. In the simplest case, the polymer structure could be represented by the formula

$$X\text{-(M-M- ..... -M-M)- Y} \quad \text{or} \quad X\text{-(M)}_n\text{- Y}$$

in which a simple straight chain composed of n units of M is terminated by two end groups X and Y. This simple formula can tell us a great deal about the polymer. X and Y may

indicate the chemistry of formation; n, the number of monomer units or degree of polymerization indicates the molecular weight and, by implication, indicates the size of the molecule. Usually n is sufficiently large that the presence of the end-groups is frequently ignored; they may however exert a pronounced effect on the properties of the polymer such as thermal stability. Their effect on electrical properties has been suggested but never clearly demonstrated.

The simplest polymer, a homopolymer, is one in which all units M are the same. Polymers containing two or more different types of structural units are called copolymers. There are three extreme types of binary (two components) copolymers, Random copolymers - ABBAABABBB have the units A and B randomly arranged along the chain. Block copolymers have groups of identical units - AAAABBBBAAAA in which the molecular weight of each block can be controlled and may be different. Alternating polymers - ABABABA have chains in which the groups alternate along the chain[17,18].

The actual polymer used in the studies presented in this thesis is an ion-exchange polymer blend and is shown in Figure 1.1. The ion-exchange polymer blend consists of a random quaternary copolymer containing two types of hydrophilic cationic groups and one hydrophobic styrene group as depicted in Figure 1.1A, mixed with poly-[(4-vinylpyridine)-co-styrene](PVP), shown in Figure 1.1B.

1.2.2 SENSITIZED POLYMERS

A. Sensitization

The effect of sensitizers on photoconduction in polymers is illustrated in the schematic shown in Figure 1.2. The effect of an organic dye is generally to introduce new regions of spectral sensitivity in addition to the regions of sensitivity which already exist in the polymer. The new regions of sensitivity correspond to the absorption spectrum of the dye. Since most dyes absorb light strongly in the visible region of the electromagnetic spectrum the net effect is to introduce photocurrent response to illumination in the visible spectrum. Since most unsensitized polymers respond mainly in the ultraviolet region, dye sensitizers generally widen considerably the spectral range of photoconductivity, e.g. produce panchromatic response. This type of sensitization has been referred to as "optical sensitization".

There is also another type of sensitization, which has been widely investigated, occurring when a polymer such as poly-N-vinylcarbazole which is a good electron donor, is doped with electron acceptor materials. This is another technique for introducing panchromatic response in the host polymer[19].

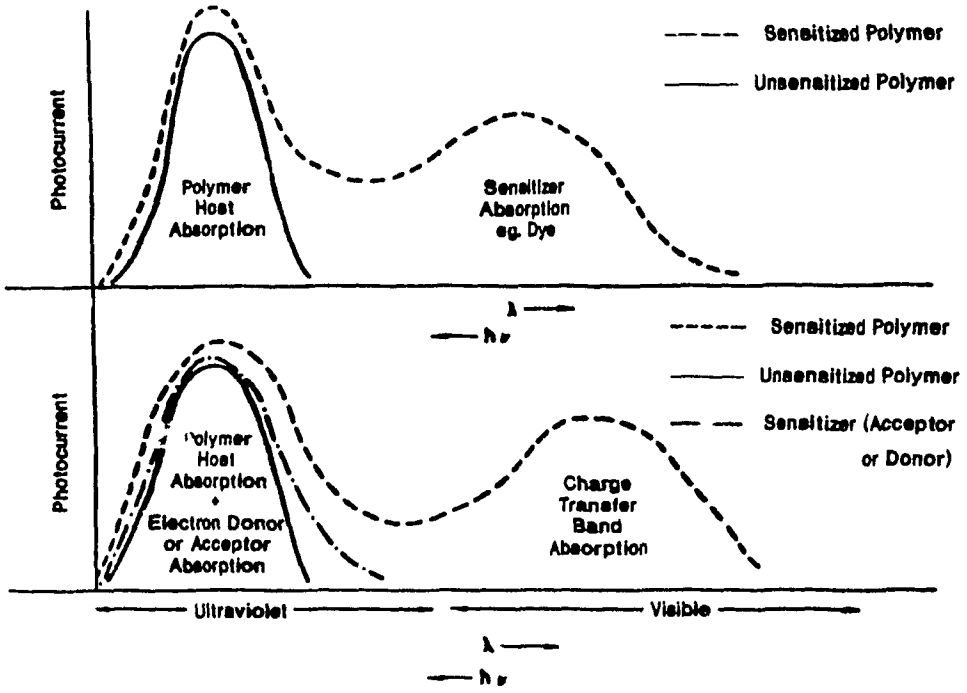

FIGURE 1.3 Effect of sensitizers on photoconduction action spectra in polymers(18)

B. Sensitizers (dyes)

Dye molecules are briefly characterized by the following properties[20]:

(1). extremely intense absorption bands in the visible region, which are due to the π (bonding orbitals)-π^*(antibonding orbitals) transitions of electrons that are present in the dye's π conjugated system.

(2). small S_1- T_1 (the singlet- triplet) intervals usually in the range 0.6 eV - 0.18 eV;

(3). triplet states normally have lower energies than the singlet states arising from the same molecular orbital configuration.

The dye, Zinc meso-tetraphenyl-porphyrin(ZnTPP), was used in our studies. The molecular structure of ZnTPP is given in Figure 1.3.

1.3 METHODS OF INVESTIGATION

There exists a variety of methods to determine the dark conductivity and the photoconductivity of organic compounds. When these methods are applied the evaluations are usually based on the band model.

1.3.1 PREPARATION OF SAMPLES

There is a variety of different techniques to prepare

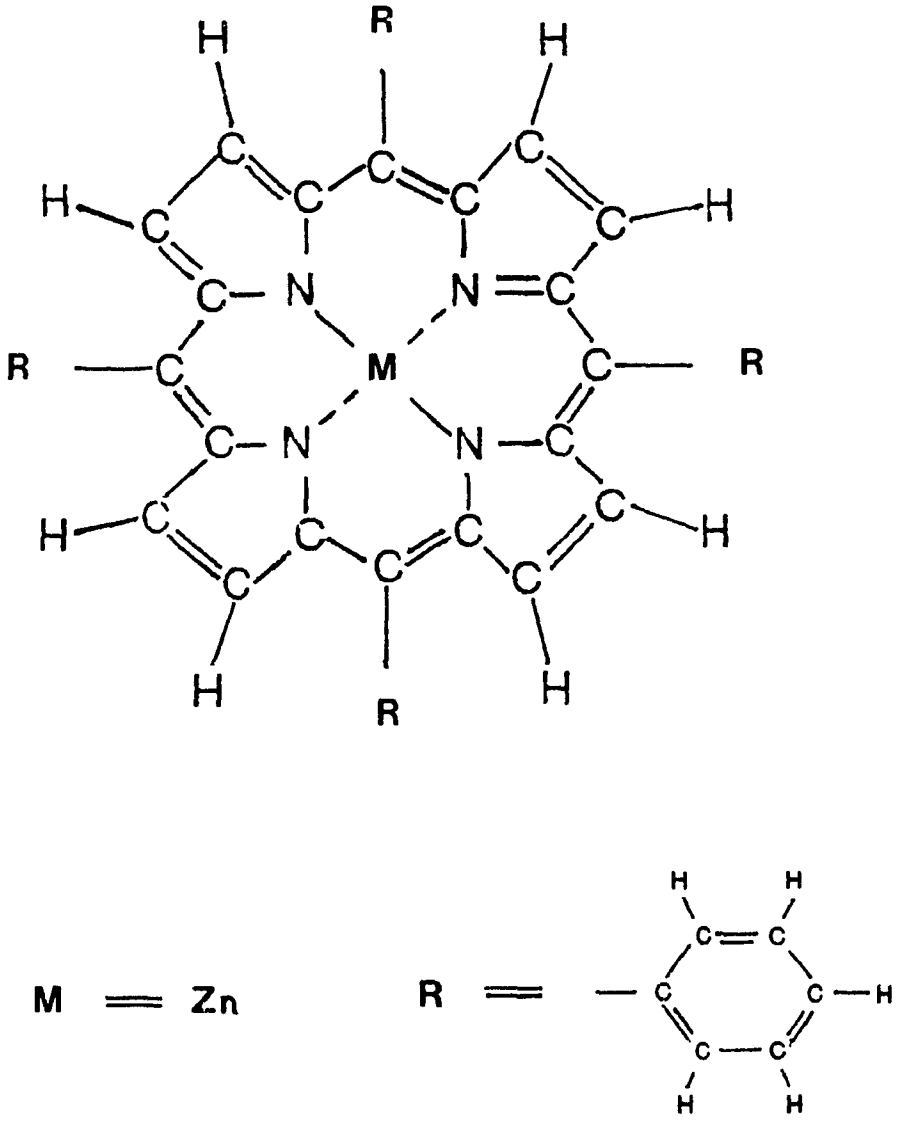

FIGURE 1.4 Molecular structure of ZnTPP

samples for investigation of the electrical properties of organic compounds. One of these techniques includes the preparation of thin films which can be obtained by solvent evaporation. This technique was used in this thesis to prepare the polymer films. In solvent evaporation, a small volume of dilute polymer solution containing the dye is deposited onto a horizontal electrode surface. The solvent is then allowed to evaporate very slowly to ensure uniform film formation. Similarly, thin films can be formed by use of Dip Coating or Spin Coating techniques[21]. These films are finally led to make sandwich cells.

Some other techniques are also employed to prepare samples such as powder sample preparation and single crystal sample preparation techniques. Powders are usually investigated in special cells in which the powders are compressed between plane electrodes [22-24]. The preparation of single crystal samples, however, usually poses a problem because most organic compounds can be synthesized only in the form of small crystals or polycrystaline powders, layers or films [25].

1.3.2 METHODS OF MEASUREMENTS

In principle, the electrical properties of organic compounds can be measured similarly to that of inorganic

semiconductors. However the measurement of the dark conductivity or photoconductivity is often difficult because of the high resistivity of many organic compounds.

A. Measurement of the dark conductivity

There are two kinds of cells which are usually employed to measure the dark conductivity, which may range from 10^{-16} to 10^{5} $(ohm.cm)^{-1}$. (a) Sandwich cells, in which the sample is located between two electrodes; (b) Surface cells, where two electrodes are applied to the surface of the sample, at a small distance from one another.

Various methods are used to obtain good contacts. These methods comprise the application of plane metallic electrodes or platinum foils on layers, crystals, etc., at a pressure of about 100 kPa/m^2 which is necessary to obtain a good enough contact for measurement[25]. A particularly useful method is the application of metal layers by evaporation(Ag,Au,Al,Pb) since in this case no additional pressure is necessary to obtain good contact [26, 27].

The design of the cell depends on the nature of the substance to be investigated (thin layer, powder, single crystal, etc.) and the property to be measured. Various designs are described in the literature[28-31]. A typical sandwich cell design can be seen in Figure 2.1 of this thesis. The cells should always be designed in such a way

that the temperature dependence of the conductivity can be determined in a temperature range as large as possible(e.g. by a resistance heater or a liquid circulation system connected with a thermometer or thermocouple). By measuring the temperature dependence of the conductivity a number of important parameters can be obtained; for example, the activation energy of the dark conductivity, ΔE, which often depends on the chemical structure of the substance, and the influence of impurities. The specific conductivity σ (ohm^{-1} cm^{-1}) can be determined from the measured sample current by means of the equation:

$$\sigma = \frac{1}{\rho} = \frac{L}{S} \frac{I_D}{V} \quad (ohm^{-1} \ cm^{-1}) \qquad (1.1)$$

where ρ is the specific resistivity (ohm cm), V is the applied voltage(V) and I_D is the dark current(A), L and S are the length (cm) and area (cm^2) of the sample, respectively.

B. Measurement of photocurrent response

The measurements are performed with the so called longitudinal field arrangements schematically shown in Figure 2.3. The longitudinal field method (sandwich cells) gives most reliable results for photoelectrical properties of an organic solid. In this arrangement the photoelectrical

behavior of the total volume of the layer between the electrodes can be studied. Furthermore, as the thickness of the film L is reduced to about 10^{-4} cm, even at low voltages, high field strengths in the sandwich cells can be achieved which enable the determination of some important trap parameters such as trap depth and the attempt-to-escape frequency . In this case one of the electrodes must be transparent. In the case of layers obtained from solution by evaporation of the solvent onto an electrode, the second electrode(metal) is applied by evaporation. Similar measurements can be performed with the surface cells (the transverse field arrangements [25, 32]).

C. Other methods of investigation

a. Contact charge exchange experiments

The basic experiment is the measurement of the film potential associated with the charge injected into the polymer film in contact with a metal. Repeated tapping contacts were found to lead to a steady state charge level in the film, and it is these levels that are important to the study of the electronic structure of the polymers[33-36].

b. Electrochemical measurements

Using photoelectrochemical cells (wet cells), both cyclic voltammetry and chronoamperometry methods have been employed

to determine the apparent diffusion coefficient of redox species which serve to give a quantitative "feel" to explain charge propagation rates in samples. Details about these methods and relevant theories can be found elsewhere[21].

1.4 REVIEW OF RELEVANT THEORIES

It should be kept in mind that the theoretical basis of many of the following concepts have traditionally depended upon long range order in the solid. In many polymers, which are amorphous or possess a low degree of crystallinity, long range order will not generally be found except possibly in one dimension.

Theoretical treatments have shown, however, that a band gap is expected between occupied and unoccupied electronic states even in amorphous solids[37]. Thus, we can assume, to first approximation, that many of the ideas developed for crystalline materials will be applicable to amorphous polymers.

1.4.1 SEMICONDUCTORS AND INSULATORS

One notices that for any semiconductor free of defects or impurities, there is a forbidden energy region in which no allowed states can exist. Above and below this energy gap

are permitted energy regions or energy bands. The upper band is called the conduction band; the lower band ,the valence band. The separation between the energy of the lowest conduction band state and that of the highest valence band state is called the band gap, E_g. The simplified band picture is shown in Figure 1.4. In this figure the bottom of the conduction band is designated by E_c and the top of the valence band by E_v.

Insulator materials at 0K have basically the same structure as that of semiconductors. The difference lies in the size of the band gap energy E_g which is much larger in insulators than in semiconductors[38].

1.4.2 DARK CONDUCTIVITY

A. Activation energy

The temperature dependence of the conductivity is given by

$$\sigma = \sigma_o \exp(- E/kT) \qquad (1.2)$$

where σ_o is the preexponential conductivity. In the case of intrinsic conductance, Eq. 1.2 can be used to calculate t e width of the forbidden energy gap, and E becomes $\Delta E/2$; for extrinsic conductance it is possible to calculate the energy of the donors or acceptors with respect to band edges, *ie,* ΔE[39-45]. These cases will be discussed in Chapter 3.

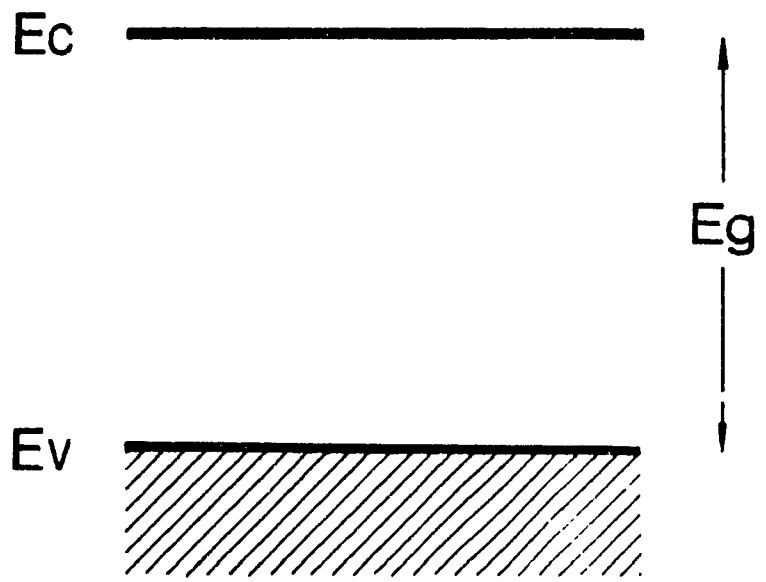

FIGURE 1.5 Simplified band structure of semiconductors

B. Space charge limited current in solids

Currents, far in excess of ohmic currents, can be drawn through thin insulators. These currents are the direct analog of space charge limited currents (SCLC) in a vacuum diode. Space charge limited currents become , therefore, a simple tool for measuring the imperfections (traps) in those insulators[46-53].

Two requirements, however, need to be fulfilled in order to observe space charge limited currents of significant magnitude: At least one of the two electrodes must make an ohmic contact with the insulator and the insulator must be in the range of low concentration of defects. The concept of an ohmic contact to an insulator is perhaps not a common one and needs to be defined. An ohmic contact is used here to mean an electrode that supplies an excess or a reservoir of carriers ready to enter the insulator as needed.

The presence of traps not only reduces the magnitude of space charge limited currents, but also is likely to distort the shape of the current-voltage curve from an ideal square law to a much higher power dependence on voltage, as shown in Figure 1.5. The particular shape can be used to determine very important parameters such as trap density and mobility. Much information can also be obtained from SCLC measurements at various temperatures.

A main advantage of SCLC measurements is that they give a direct image of the presence or absence of traps in the

solid. SCLC measurements can also be used to distinguish between a monoenergetic trap level and an exponential trap distribution, however, the whole current voltage characteristic for the trap distribution can be much more complicated than the one shown in Figure 1.5.

1.4.3 THEORY OF ISOTHERMAL DECAY CURRENTS

Most of the theoretical work done to date is such that it is useful to analyze the experimental data only when an *a priori* knowledge of the trap distribution exists, since the nature of the trap distribution is not apparent from the experimental data *per se*. But the theory of isothermal decay currents developed by Simmons and Tam can be used to determine trap parameters in semiconductors and insulators containing arbitrary trap distributions without an *a priori* knowledge of the trap distribution[54-72].

Simmons and co-workers studied the isothermal time-dependent current characteristics obtained for semiconductors and insulators containing arbitrary trap distributions when the applied electric field is sufficiently high, and the active region in which the free carriers are generated optically or electrically is sufficiently thin, so that recombination of free carriers is

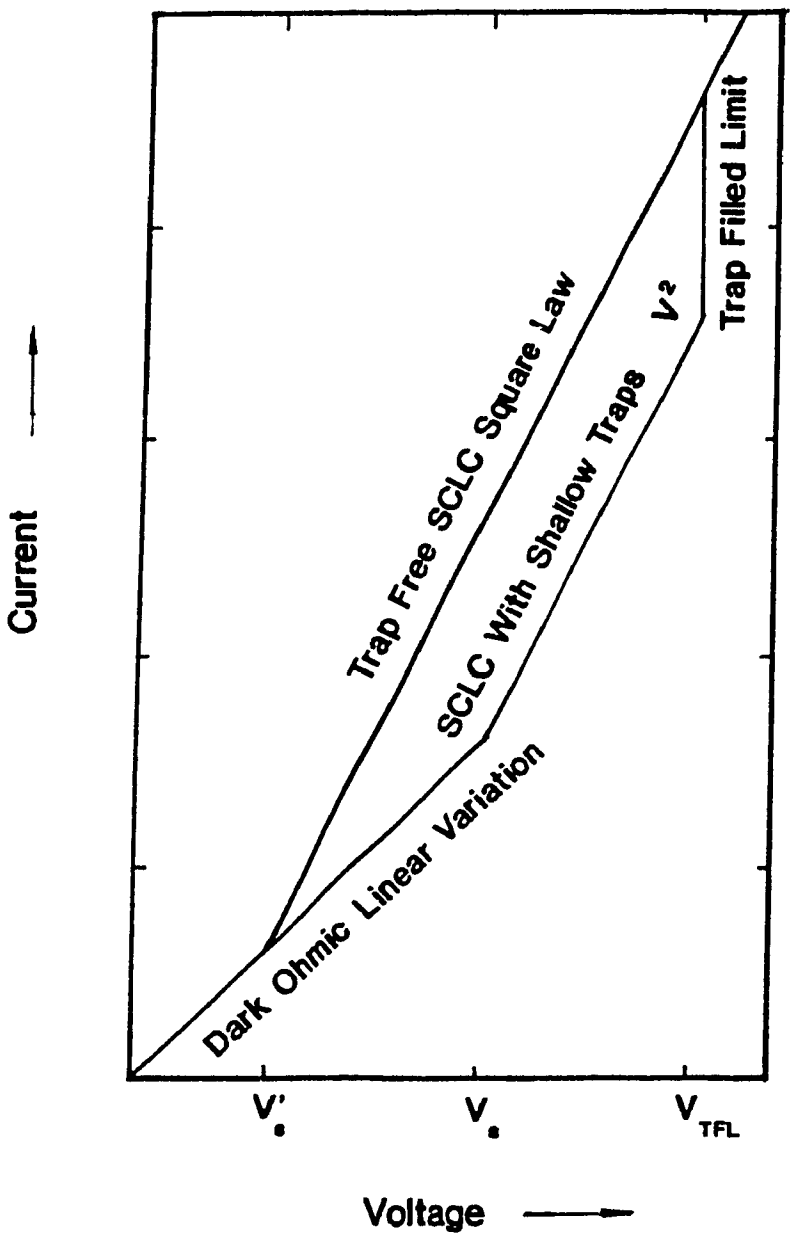

FIGURE 1.6 A prototype of steady state I - V characteristics for a solid(19)

negligible. This occurs, for example, in reverse-biased p-n junctions, Schottky barriers, and thin-film insulators and semiconductors, under appropriate biasing conditions. Under these conditions, they have shown that the current-time(I-t) characteristics can be obtained in closed form for any trap distribution. More important, however, they have shown that when the high-field isothermal data are plotted in the form of an It-vs-$\log_{10}$(t) characteristic, the shape of the characteristic then provides a direct means of determining the trap distribution and some other trap parameters.

1.4.4 MOLECULAR ION STATE MODEL APPROACH

In disordered organic solids, electron transport over any distance in the field direction occurs by the so-called hopping mode. This requires intermolecular electron transfer via weak Van der Walls interaction. The weakness of the intermolecular binding forces in polymeric solids causes the electronic states of the solid to derive from the positive and negative molecular ion states of the isolated molecules rather than from Bloch states, as in covalent crystals.

In analogy to semiconductor band theory, a neutral acceptor state or an ionized donor state will trap an electron, and a neutral donor state or ionized acceptor state will trap holes. Duke and Fabish have described

localized states for pendent-group polymers in terms of a molecular ion model[33-36,73-78]. The electronic structure of the polymer is basically that of an ensemble or group of molecular subunits since the bandwidth due to overlap of pendant groups is so small. In an effort to understand these molecular ion states Duke and Fabish performed metal-polymer contact charging experiments. They measured the charge transferred to polymers from metals with different work functions. The results suggest that each metal transferred charge only to particular polymer states which were localized in a narrow window (about 0.4 eV) near the metal Fermi level.

The molecular ion state model for pendant group polymers can be represented as a Gaussian distribution composed of acceptor states (E_{anion}) and donor states (E_{cation}) as shown in Figure 1.6. The relative intensities of the bands is a measure of the bulk density of states. These bands should be regarded as broad continuous distributions of donor and acceptor states, in which injected charges can travel by a hopping mechanism from one state to another as shown in Figure 1.7. It would therefore be more favorable for charge transport processes to inject electrons into acceptor states of high density. These molecular ion states were calculated from contact charge exchange measurements between metal surfaces and polymers, and it is not known how the shape and position of these levels might be influenced

under visible or UV-illumination.

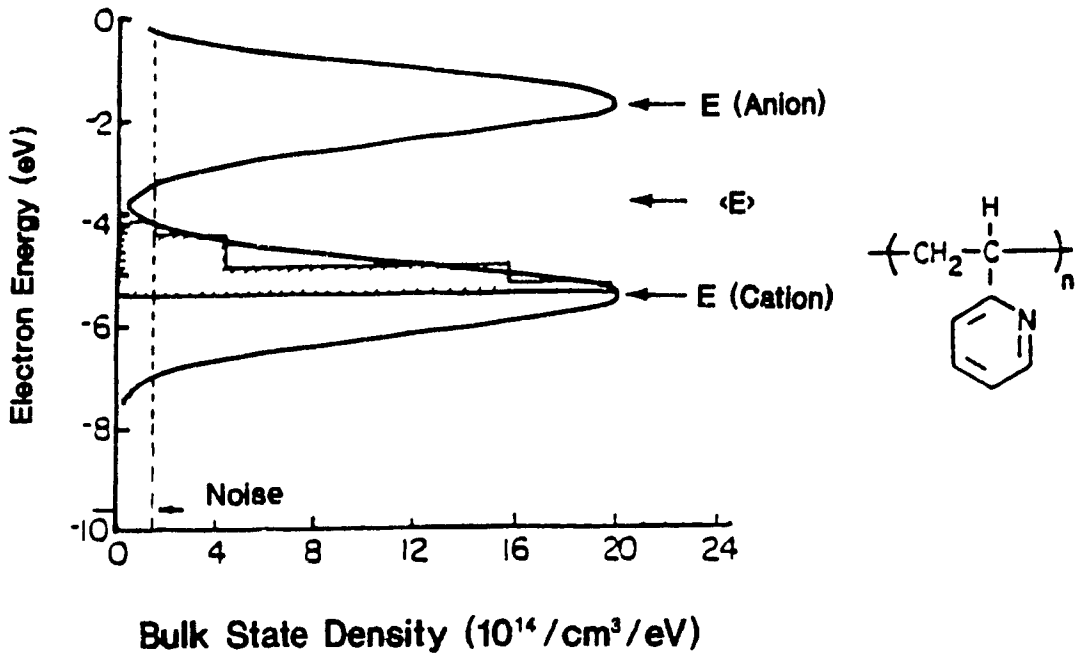

FIGURE 1.7 Continuous Gussian distributions of molecular ion state energies for poly(2 - vinylpyridine) as determined from contact charge exchange experiments

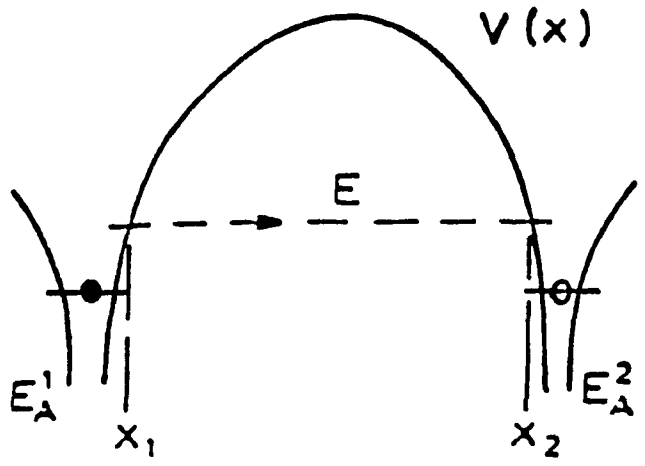

FIGURE 1.8 Electron tunnelling through a barrier V(x) at energy E from an occupied acceptor state E_A^1 to an empty acceptor state E_A^2 (35)

CHAPTER 2

EXPERIMENTAL METHODS

The principal aim of the experimental program was to cast the polymer films witn or without the dye and make the following measurements:

a) the dark current vs. voltage

b) the dark current vs. temperature

c) the complete photocurrent profile

2.1 SAMPLE PREPARATIONS

2.1.1 PREPARATION OF RANDOM COPOLYMER

The random ternary copolymer was prepared according to a modification of the procedure developed by Montgomery and Anson[2, 3]. The monomers, 8.1g vinyl benzyl chloride (Kodak Eastman Co.) and 1.7g styrene (Aldrich Chemical Co.) were dehibited and then diluted to about 110 ml in benzene. AIBN (0.9g Aldrich, recrystallized in ethanol) was added and the solution was degassed thoroughly with nitrogen gas for two hours. The polymerization was then allowed to proceed at 60 ^{0}C for 24 hours under a blanket of nitrogen. Then the

solution was slowly added to methanol. The styrene-chloromethylstyrene copolymer was collected by vacuum filtration.

Quaternization of the chloromethylstyrene moiety of the copolymer was carried out via the Menschutken reaction(14). The precipitate was redissolved in benzene and a 10-fold molar excess of triethylamine (Aldrich Chemical Co.) was added. The resulting solution was refluxed at 80 ^{0}C for 1.5 hours and then allowed to cool. This was followed by addition of a 10-fold molar excess of triethanolamine (Aldrich) and refluxed for an additional 1.5 hours. A yellowish sugary precipitate was obtained at the bottom of the flask. The benzene was decanted and the remaining solid was washed with more benzene, discarding the washings. The solid was dissolved in spectrograde methanol (Caledon) and preconcentrated by rotoevaporation. This solution was then added to a stirred solution of isopropanol with a pasteur pipette to precipitate the quaternary copolymer. The product was collected by vacuum filtration. A 2% (w/v) working solution was prepared by dissolving the quaternized copolymer in methanol[16,17,21].

2.1.2 PREPARATION OF POLYMER BLEND

Poly [(4-vinylpyridine)-co-styrene], styrene content 10% (PVP, Aldrich Chemical Co.), shown in Figure 1.1 was used as received and dissolved in methanol to give a stock solution of 2% PVP w/v. Equal volumes of PVP and random quaternized copolymer solutions were thoroughly mixed together to constitute the polymer blend also referred to below as polyXIO for simplicity.

2.1.3 PREPARATION OF DYE-POLYMER BLEND (ZnTPP/POLYXIO)

ZnTPP(75 mg, Strem Chemicals, Inc.) dissolved in 10 ml of methanol was added to 20 ml of the PVP-copolymer blend solution described above. The solution was stirred using a magnetic stirrer for 2 hours to give the polymer blend solutions with ZnTPP dye. All solution were stored in the dark. The solvent, methanol, was of spectrograde quality (Caledon, Anachemia).

2.1.4 PREPARATION OF SnO_2 ELECTRODES

Rectangular SnO_2 optically transparent electrodes(OTE) (1.5 × 5.0 × 0.32 cm) were cut from SnO_2 coated infra-red

reflective (I-R-R) pyrex plates (Swift Glass Co.). The SnO_2 OTE's had typical resistances of about 30 ohms/cm. Prior to use they were soaked in sulfochromic acid (Chromerge, Fisher) for 20 mins. After being thoroughly rinsed with distilled water, the electrodes were dried in a stream of prepurified nitrogen gas.

2.1.5 PREPARATION OF ZnTPP/POLYXIO FILMS

Films were cast on the SnO_2 OTE's by solvent evaporation of the prepared solutions. Film thickness was varied by depositing 0.1 - 1.0 ml of solution depending on the thickness desired. All the electrodes were prepared under an inverted crystallization dish in the presence of $CaCl_2$ and placed on a perfectly level plate to ensure uniform films. Typical film thicknesses obtained in this manner were about 5 μm by depositing 0.27 ml of the solution. After the film had dried, one third of the total film area was wiped off with use of methanol. Nail polish was then applied over the boundary between the polymer film edge and the part where the polymer was removed, and acted as an insulator between SnO_2, and the gold film to be evaporated over the polymer film.

A thin film of gold was coated onto the selected surface of the modified SnO_2 electrodes by vacuum evaporation at

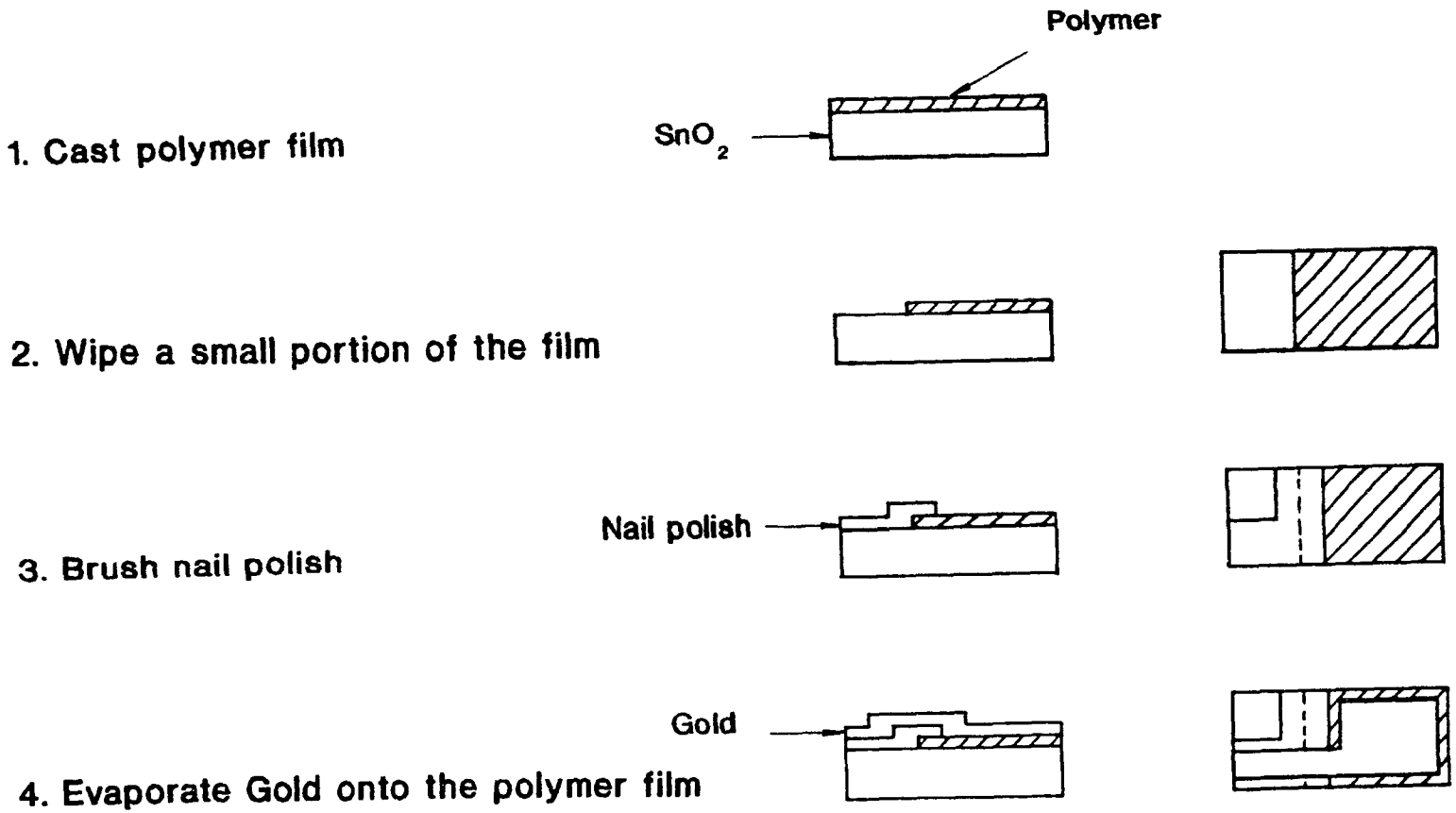

FIGURE 2.1 Steps in the fabrication of the sandwich cell with the dye/polymer blend in the middle

10^{-7} Torr (Varian VK12B cryogenic pump). The selected surface was made by using Scotch tape to mask the unwanted surface area. The SnO_2 and gold contacts were connected using wires and silver paint producing a "Sandwich" cell(see Figure 2.1).

2.2 APPARATUS AND PROCEDURES

2.2.1 ABSORPTION SPECTRA

Absorption spectra of all solid state samples were taken with a HP8452 UV-vis diode array spectrophotometer. Solid state spectra were obtained by mounting the dye/polymer blend modified SnO_2 OTE's in front of the spectrophotometer cell holder. An appropriate blank was employed in all cases to correct for background signal (i.e., a bare SnO_2 OTE was used for all ZnTPP/polyXIO/SnO_2 samples.)

2.2.2 FILM THICKNESS MEASUREMENTS

Surface profile measurement of the dye/polymer blend films on the SnO_2OTE substrate were done mechanically using the Talysurf Taylor-Hobson Step Profilometer. A hand-held micrometer (Mitutoyp) was also used for thicker films. A portion of the film was wiped off with methanol to expose a

portion of SnO_2 substrate leading to the step to measure film thickness.

2.2.3 LIGHT INTENSITY MEASUREMENTS

The light intensities of the radiation sources were measured with a radiometer/photometer (Model 88XLC) which was equiped with a Model 400 sensor head. All readings were calibrated by using the table of Calibration Certification for the Model 88XLC.

2.2.4 SOLID STATE CELLS

A. Experimental setup

The schematic experimental arrangement used for all measurements is illustrated in Figure 2.2. A Keithley (Model 617) programmable Electrometer was used as both the voltage source and the current or resistance recorder. The current at various applied voltages and temperatures was also monitored by coupling the electrometer to a strip chart recorder. Monochromatic illumination was obtained by using a 150W Xenon lamp and a manual/motor driven monochromator (Bausch and Lomb). The cells were encased in a sealed pyrex glass container with an inlet and outlet allowing for nitrogen gas purging. The glass container was placed in a

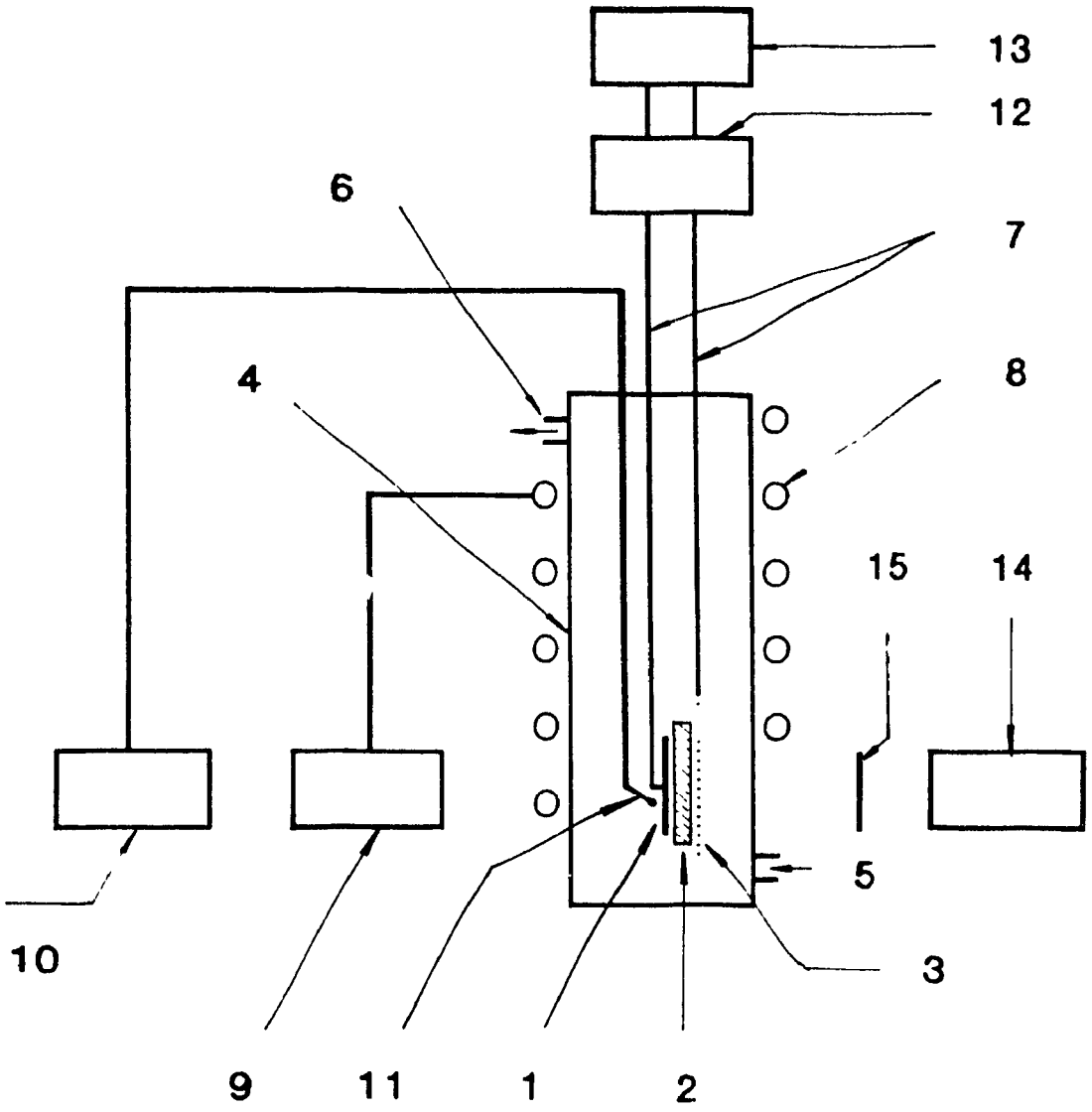

FIGURE 2.2 Schematic experimental arrangement for D.C. dark and photoconductivity studies

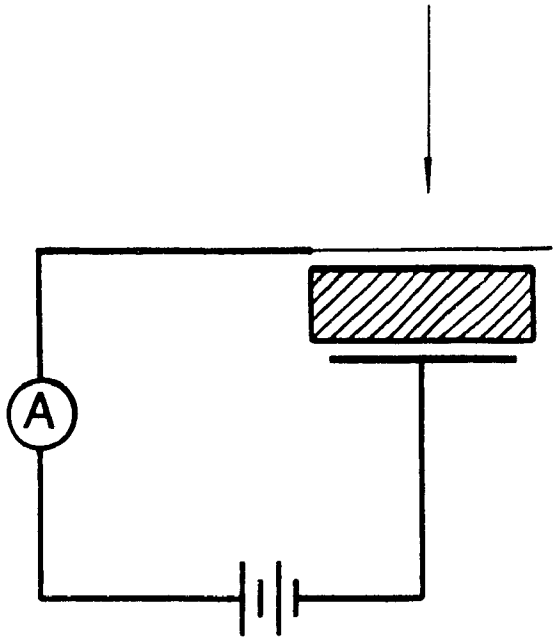

FIGURE 2.3 Schematic diagram for photocurrent measurements

metal box which had a window allowing light to illuminate the samples. The metal box is not shown in Figure 2.2 and only the position of the shutter is shown. Flexible heating tape was wrapped around the glass container in order to change the temperature of the cell, and a thermocouple was employed to monitor the change in temperature. All measurements were done in an inert gas atmosphere, nitrogen. All conductivity(electrical) measurements were taken after the cell was purged with nitrogen for many hours(overnight) and the dark current had stabilized.

There were two major parts in the experimental program. Part 1 dealt with the influence of the voltage and temperature on the dark conductivity of the polymer, with or without dye. Part 2 dealt with the determination of some trap parameters by considering the variation in photocurrent of the dye polymer films with respect to time at different voltages, at different temperatures, or different light intensities.

B. Description of equipment

The various sets of equipment used in this project (shown in figure 2.2) were:

a) Sandwich cell (the dry cell)

(1) Evaporated Au film

(2) PolyXIO or ZnTPP/polyXIO film

(3) SnO_2 optically transparent electrode (OTE)

b) Glass container

(4) Cylindrical shape glass container (which consists of two parts, the top part and the bottom part, held together by a metal clamp.)

(5) Gas inlet

(6) Gas outlet

(7) Two brass sample holders (which also enable the cell to be connected to the electrometer.)

c) Heating and cooling system

(8) Flexible heating tape or plastic tubing (with the circulation of a mixture of water, salt and ice in it)

(9) Variable autotransformer or a reservoir (of the cooling mixture)

d) Temperature monitoring devices

(10) OMEGA HH-52 Hand held digital thermometer

(11) Thermocouple

e) Current measuring devices

(12) Electrometer (Keithley Model 617 programmable electrometer) including a built in voltage source. The measuring range of the Model 617 is between 10μV and 200V for voltage measurements, 0.1fA and 200mA in the current mode, 0.1Ω and 200Ω (up to 10^{16} Ω using the built in voltage source in the V/I mode)

(13) Strip chart Recorder

f) Light source

(14) Bausch & Lomb high intensity Monochromator, 150 watt Xenon lamp with Power Supply and a cooling fan

(15) Shutter

CHAPTER 3 RESULTS AND DISCUSSION

3.1 DARK CONDUCTIVITY

In this section we begin to probe the energy gap, and the position of trap levels in the forbidden zone, as well as the influence of traps on the carrier mobility in the polymer (polyXIO) by measuring of the voltage dependence of the dark current and the temperature dependence of the dark conductivity. It was found that the traps present are associated with the polymer and are not significantly influenced by the presence of the dye.

3.1.1 VOLTAGE DEPENDENCE OF THE DARK CURRENT

The typical dark current-voltage curves of polyXIO alone and ZnTPP/polyXIO on SnO_2 OTE are shown in Figure 3.1, the dark currents, I_D, at field strengths of 10^2 to 10^4 V cm^{-1}, vary with increasing voltage according to

$$I_D = a\ V^S \qquad (3.1)$$

where V is the applied voltage and a is a constant. The

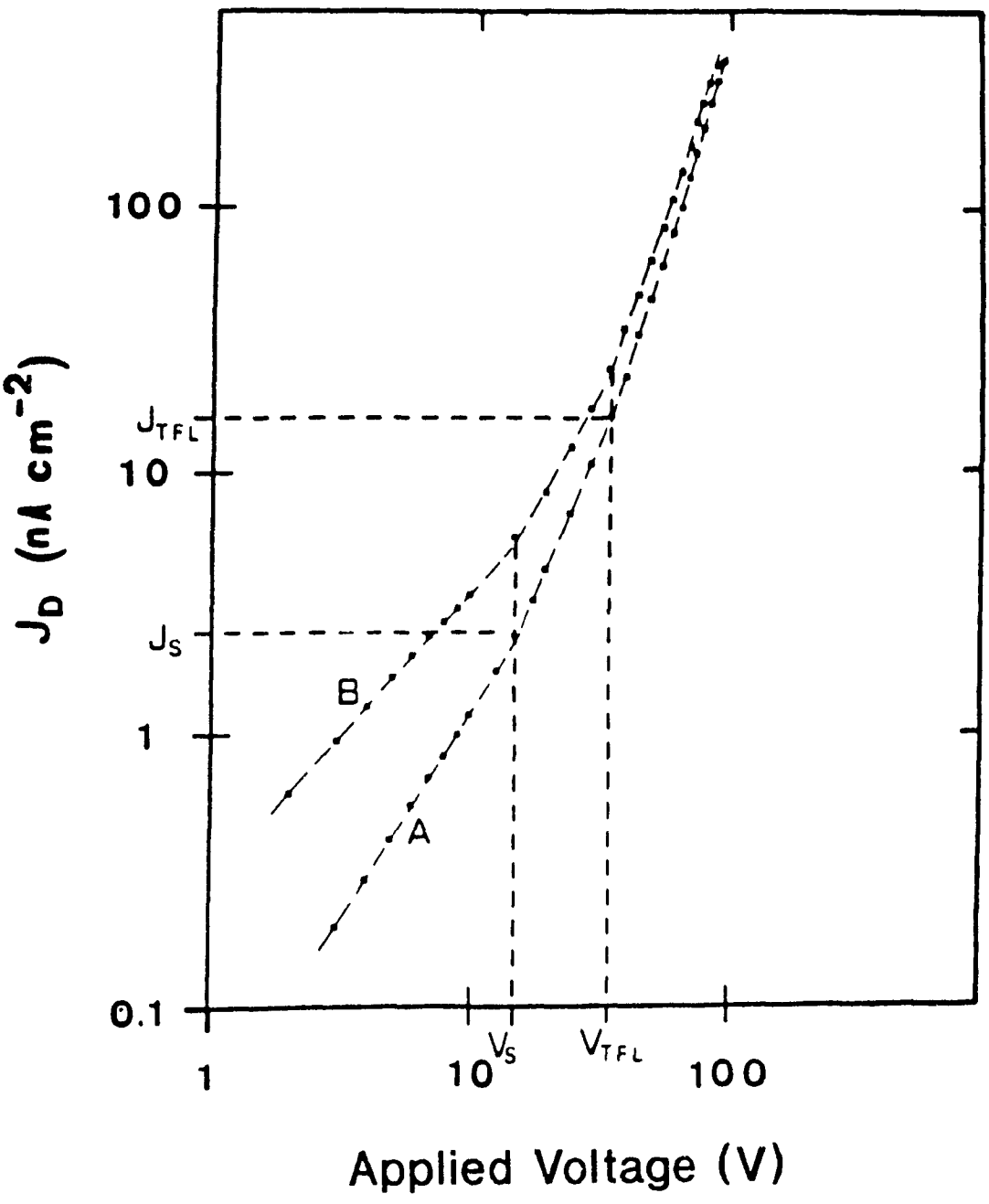

FIGURE 3.1 Dark current vs. applied voltage

A: polyXIO only and B: ZnTPP/polyXIO

parameter s was found to have values of 1.0 to 1.3 in the ohmic region, 1.9 to 2.2 in the SCLC region, and 2.8 to 3.0 in the trap filled region. These results possess the general characteristics predicted by the Rose-Lambert theory[46,47]. There are two important regions. The region between V_0 (zero voltage) and V_S corresponds to the ohmic region. V_S is defined as the voltage at which the number of injected carriers is equal to the thermal equilibrium carrier density of the material. At these low applied voltages, the rate at which carriers are supplied into the solid is equal to the rate of their departure by drift at the opposite contact. In this region, the dark current is linearly dependent on the applied voltage, and ohm's law holds.

The second region, between V_S and V_{TFL}, is known as the space charge limited (SCL) region. At these higher applied voltages, the carriers injected into the solid overcome the requirements for ohmic current considerations, therefore, at any instant, the carrier density in the solid is larger than the value that existed prior to the application of the voltage. The drift of this excess space charge results in a current that is higher than the ohmic current and is called the space charge limited current (SCLC). The current-voltage characteristic in this region is given by Child's law [25]

$$I_D = \frac{9\ F\ \varepsilon\ \varepsilon_o\ \mu\ V^2}{8\quad L^2} \qquad (3.2)$$

Where ε is the relative dielectric constant, ε_o the permittivity of free space, L the sample thickness, and F the electrode surface area. The dielectric constant, ε , for the medium was taken to be 3 which is common for most polymer materials(19). μ is the drift mobility. Since an injected (or thermally generated) carrier is influenced during its migration through the solid by multiple trapping and detrapping events, the microscopic mobility μ_o, which depends on the band width and the effective mass, respectively, has been replaced by the smaller drift mobility

$$\mu = \varnothing\ \mu_o \qquad (3.3)$$

where $\varnothing$ is the fraction of free to trapped carriers(see Eq.3.6).

Therefore, the drift mobility can be derived from the slope of the I_D- V^2 curve(35,36), $dI_D/\ d(V^2)$ shown in Figure 3.2.

$$\mu = \frac{[\ 8\ L^3\ dI_D/\ d(V^2)\ ]}{9\ \varepsilon\ \varepsilon_o\ F} \qquad (3.4)$$

The drift mobilities of polyXIO alone and ZnTPP/PolyXIO are $3.1 \cdot 10^{-9}$ $cm^2V^{-1}s^{-1}$ and $4.1 \cdot 10^{-9}$ $cm^2V^{-1}s^{-1}$ respectively. The mobilities are very close to each other in the systems with or without dye and are not significantly influenced by the presence of the dye. The low mobility suggests that charge transport occurs by a hopping mechanism operating between localized pendant groups, for example, between pyridine groups. The type of behavior observed for both systems(Figure 3.1), with a region where current is proportional to the voltage squared. is in fact the characteristic of an insulator containing traps.

When the voltage reaches V_{TFL} the voltage at which the traps are filled, the current rises even more rapidly and is proportional to $V^{>3.8}$. V_{TFL} is the voltage at which the trap filled limit(TFL) is reached. At the trap filled limit, the total density of traps, N_t, present in the polymer or dye/polymer film, is given by[25]

$$N_t = \frac{9\ \varepsilon\ \varepsilon_o V_{TFL}}{8\ e\ L^2} \qquad (3.5)$$

where e the charge of the electron.

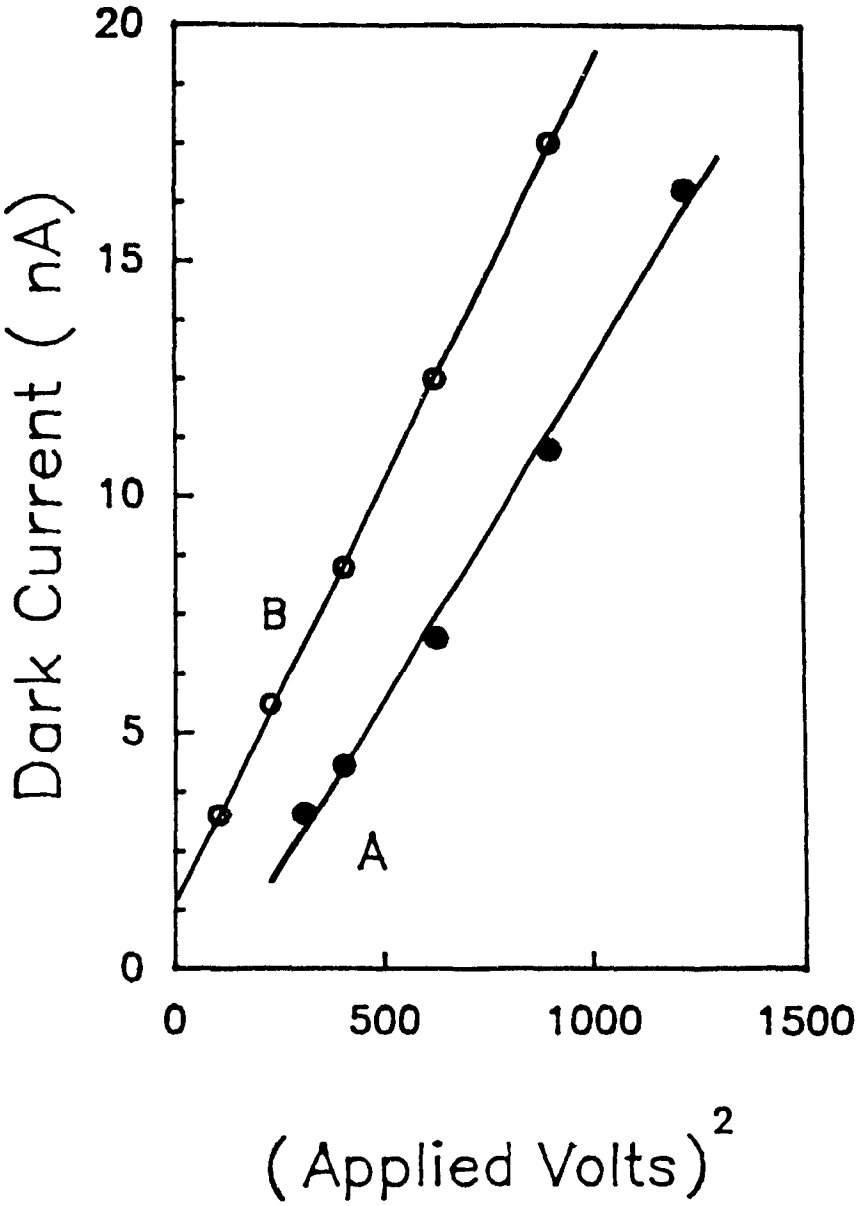

FIGURE 3.2 Dependence of dark current on applied voltage in SCLC region A: polyXIO alone and B: ZnTPP/polyXIO

From the results presented in Figure 3.1, the trap filled limited voltage (V_{TFL} = 40 V) was found to be the same for both polyXIO alone and ZnTPP/polyXIO. Using the experimentally obtained V_{TFL}, the density of trap states, N_t, was calculated to be about 10^{14} states/cm^3. Here again the trap states are believed to be associated to the polymer instead of the dye because V_{TFL} was approximately equal in the systems with or without dye. This total trap density is less than the maximum charge density which was experimentally observed by the contact charge experiments of Fabish and Duke which amounts to 4 $\times$ 10^{15} states/cm^3 [26].

In the case of shallow traps near the conduction band or valence band, there exists a thermal equilibrium between free (n, p) and trapped (n_t, p_t) carriers, which depends on the depth of the traps, $\Delta E_{t(n)} = E_C - E_t$ and $\Delta E_{t(p)} = E_t - E_V$, the trap concentrations N_t, P_t, and the effective density of states in the conduction band, N_C, and valence band, N_V. The fraction $\varnothing$ of free carriers to trapped carriers is given by

$$\varnothing_n = \frac{N_C}{N_t} \exp \left(- \frac{\Delta E_{t(n)}}{k\ T} \right) \qquad (3.6A)$$

$$\phi_p = \frac{N_V}{P_t} \exp\left(-\frac{\Delta E_{t(p)}}{k\,T}\right) \qquad (3.6B)$$

where $\phi_n = n / n_t$ and $\phi_p = p / p_t$ under the conditions that $n_t \gg n$ and $p_t \gg p$. For shallow monoenergetic traps with a concentration of $N_t = 10^{14}$ cm^{-3} and $E_t = 0.81$ eV (see chapter 4) we obtain (with $N_C = 10^{21}$cm^{-3}) $\phi = 10^{-7}$. The results are summarized in Table 3.1

TABLE 3.1 SOME ELECTRICAL PARAMETERS OF POLYXIO ALONE AND ZnTPP/POLYXIO

	V_S(V)	V_{TFL}(V)	μ (cm^2/Vs)	N_t(cm^{-3})	ϕ
PolyXIO	18	40	$3.1\cdot10^{-9}$	10^{14}	10^{-7}
PolyXIO/ZnTPP	18	40	$4.1\cdot10^{-9}$	10^{14}	10^{-7}

The trap depth ΔE_t can also be determined experimentally

from the SCLC region. Eq. 3.2 can be rewritten as follows[25]

$$I_D = \frac{9}{8} F \varepsilon \varepsilon_o \mu_o \frac{V^2}{L^3} \left[\frac{N_c}{N_t} \exp \left(- \frac{\Delta E_t}{k T} \right) \right] \qquad (3.7)$$

A plot of ln I_D vs. 1/T at V = const. yields the trap depths $\Delta E_{t(n)}$ or $\Delta E_{t(p)}$ (shown in Figure 3.3). $\Delta E_{t(1)}$ is found to be 0.73 eV and $\Delta E_{t(2)}$ is 0.45 eV (see Table 3.2). The trap depth, $\Delta E_{t(2)}$ will be discussed in the next section.

TABLE 3.2 ACTIVATION ENERGIES AT VARIOUS APPLIED VOLTAGES (In The Space Charge Limited Region)

Applied Voltages(V)	$\Delta E_{t(1)}$(eV)	$\Delta E_{t(2)}$(eV)
22	0.72	0.40
25	0.73	0.47
32	0.75	0.48
Average	0.73	0.45

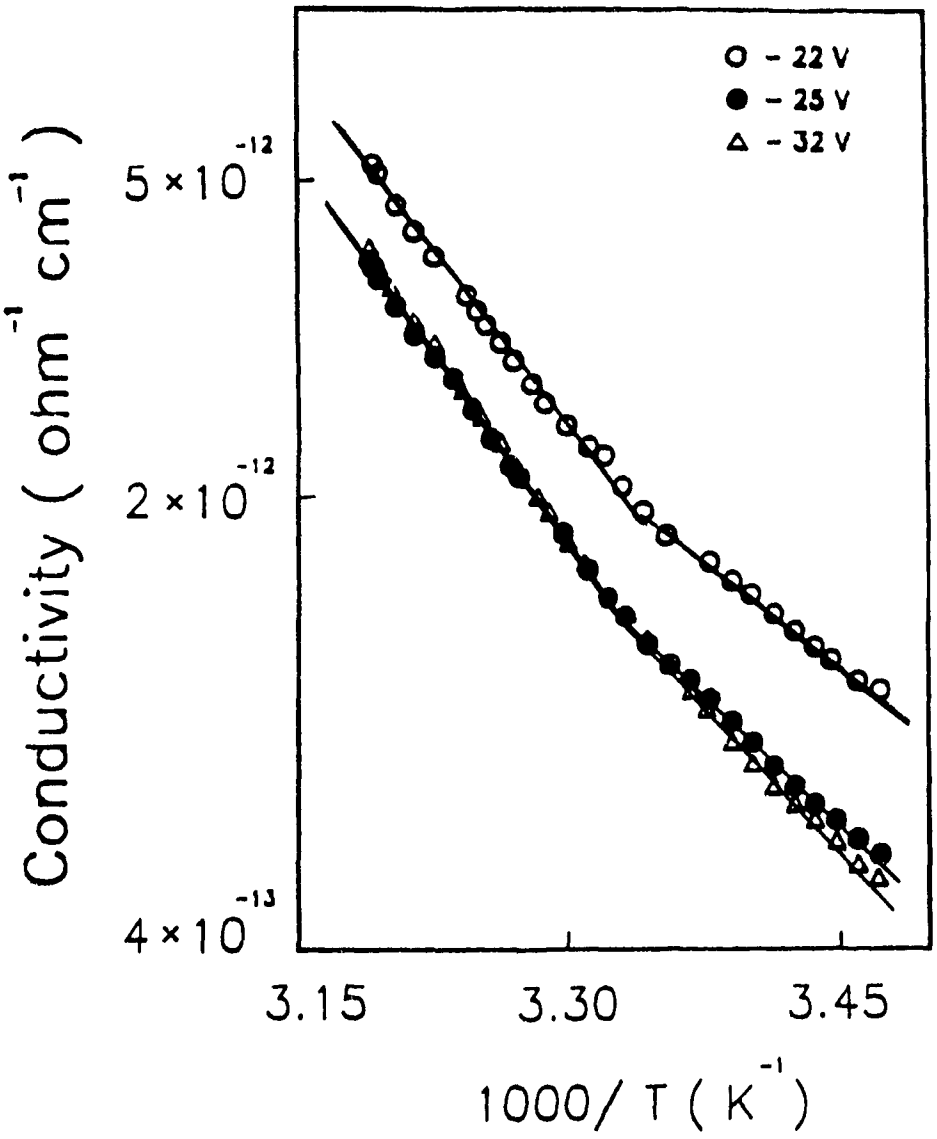

FIGURE 3.3 Temperature dependence of conductivity of ZnTPP/polyXIO system at SCLC region

3.1.2 TEMPERATURE DEPENDENCE OF THE DARK CONDUCTIVITY

The electrical behavior of many organic systems can be explained by the laws of semiconductor physics. This section will use some of these basic principles to interpret our experimental results. As we know, a non-irradiated semiconductor with a fully occupied valence band and empty conduction band can become conducting under the influence of thermal lattice vibrations. Either electrons are lifted from the valence band to the conduction band or electrons (or holes) are excited from defects. In the first case we speak of intrinsic conductivity, in the second case of extrinsic conductivity.

A. Polymer alone (Intrinsic conductance)

A general relation for the temperature dependence of the conductivity of an intrinsic semiconductor is

$$\sigma = \sigma_o \exp\left(- \frac{\Delta E}{2 k T} \right) \qquad (3.8)$$

Where ΔE is the width of the forbidden gap ($\Delta E = E_c - E_v$). So that by plotting $\ln\sigma$ versus $1/T$, the slope of the

straight line, $\Delta E/2k$. gives the width of the forbidden gap. Figure 3.4 shows the temperature dependence of dark conductivity of polyXIO alone and ΔE was found to be about 4.0 eV.

B. Polymer with Dye (mixed conductance)

For the mixed conductance the total conductivity of a semiconductor results from both intrinsic and extrinsic conduction:

$$\sigma = \sigma_o \exp\left(-\frac{\Delta E}{2 k T}\right) + \sigma_{o(ex)} \exp\left(-\frac{\Delta E_t}{k T}\right) \qquad (3.9)$$

A plot of $\ln\sigma$ vs. (1/T) yields different straight lines which depend on ΔE and ΔE_t ($\Delta E_t < \Delta E$). Only after an excitation of all defects (traps) can the width of the forbidden gap $\Delta E = E_c - E_v$ be determined from the temperature dependence of the conductivity(16,37). From Figure 3.5 values of ΔE = 4.0 eV and ΔE_t = 1.5 eV were found.

B. Extrinsic conductance

The temperature dependence of the conductivity of an extrinsic semiconductor is given by

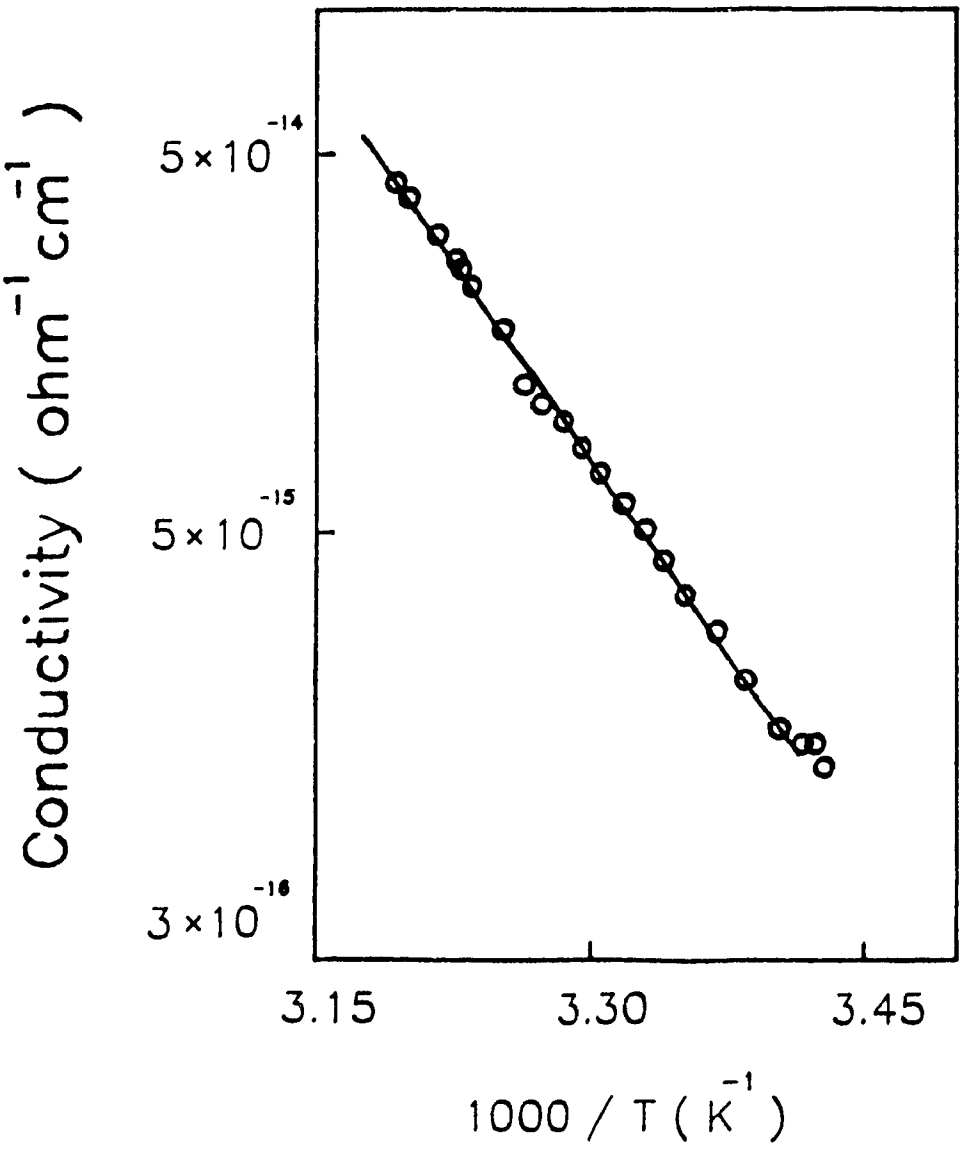

FIGURE 3.4 Temperature dependence of conductivity of polyXIO alone

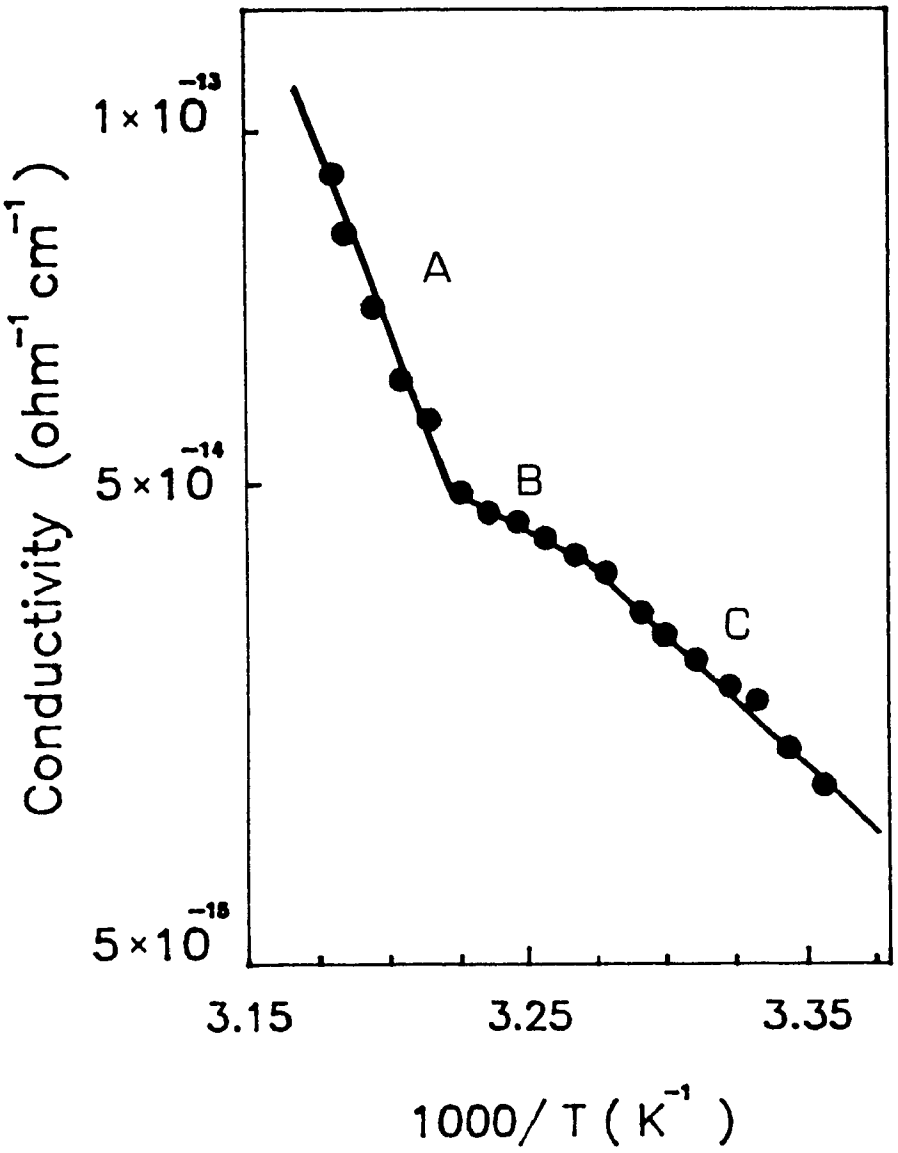

FIGURE 3.5 Temperature dependence of conductivity of ZnTPP/polyXIO system

$$\sigma = \sigma_{o(ex)} \exp\left(-\frac{\Delta E_t}{k\,T}\right) \qquad (3.10)$$

where $\Delta E_{t(n)} = E_c - E_t$ or $\Delta E_{t(p)} = E_t - E_v$ (see figure 3.6). ΔE_t can be obtained in the same way described for the intrinsic case. The activation energies are listed in the Table 3.2.

TABLE 3.3 ACTIVATION ENERGIES AT VARIOUS APPLIED VOLTAGES

Applied Voltages(V)	ΔE_t (eV)
0.2	1.52
0.4	1.51
0.6	1.59
Average	1.54

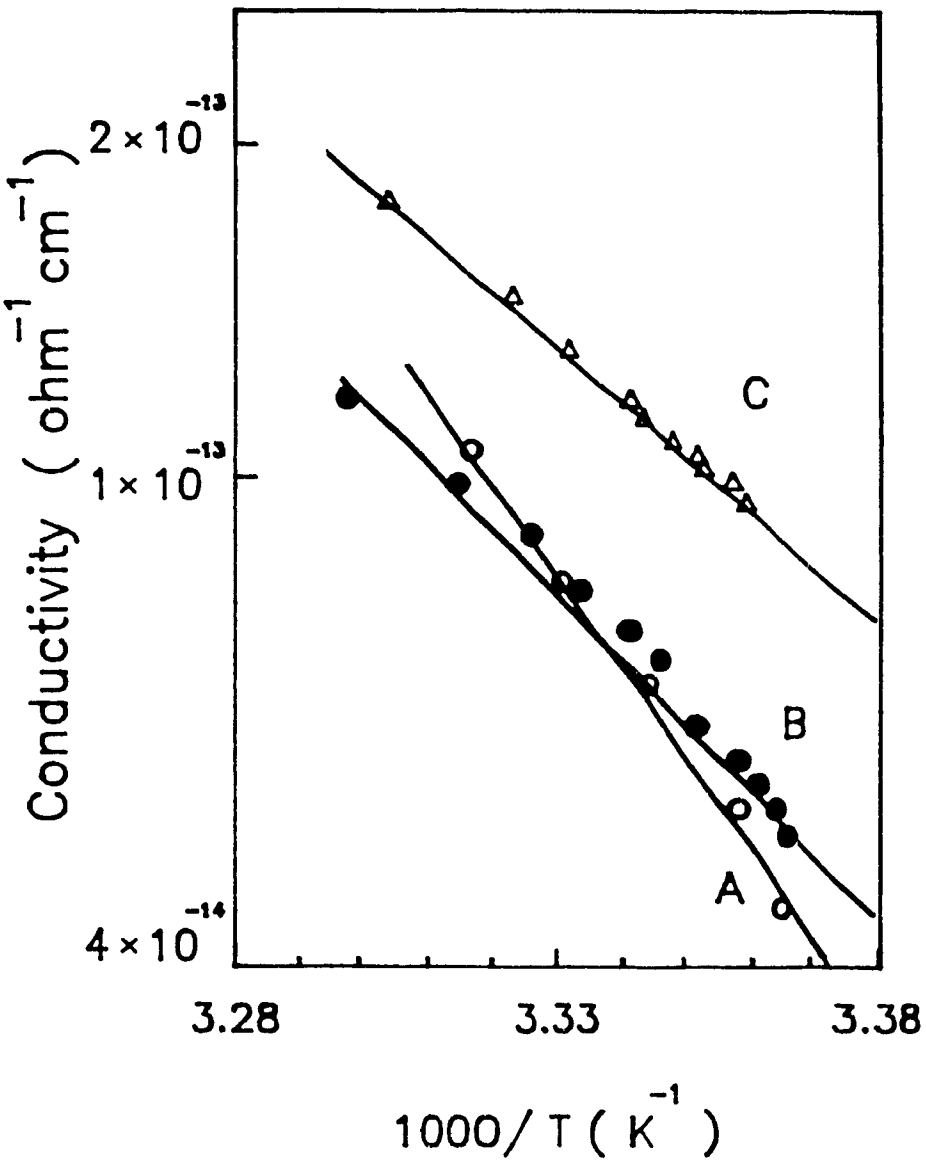

FIGURE 3.6 Temperature dependence of conductivity of ZnTPP/polyXIO system (A: 0.2V, B: 0.4V, C: 0.6V)

3.1.3 COMMENTS ON THE CONDUCTANCE MECHANISMS

Figure 3.5 shows that the temperature dependence of the conductivity is in agreement with the above theory although we are dealing with insulators (amorphous polymer materials) rather than semiconductors. In other words, to a certain extent, this polymer/dye system behaves like a band semiconductor with traps. In Figure 3.5, region A corresponds to intrinsic conductance, region B to defect exhaustion and region C to extrinsic conductance. We found ΔE and ΔE_t to be 4.0 eV and 1.5 eV respectively. Compared with Figure 3.4, it is obvious that the ΔE_t of 1.5 eV is associated to the presence of ZnTPP because this trap level is not observed in polyXIO alone. For the temperature dependence of the dark conductivity, the broader the temperature range the more reliable the results. A mixture of water, salt and ice was used to lower the temperature down to around 0°C and a flexible heating tape was used to raise the temperature to 45 °C. Unfortunately, the dark current was unmeasurable at temperatures below 10°C. Nevertheless, various samples which were cast in the same way were used to make these measurements and the results are very consistent (shown in Table 3.4).

TABLE 3.4

ACTIVATION ENERGIES OF VARIOUS SAMPLES OF ZnTPP/POLYXIO

Sample No.	ΔE (eV)	ΔE_t (eV)
1	4.0	1.5
2	3.8	1.5
3	3.9	1.5

The thermal activation energy, ΔE, which was obtained from the temperature dependence of the dark conductivity is not an unambiguous quantity since various processes may cause conductivity. Some of these processes will be discussed below. From the voltage dependence of the dark current, the dark current of polyXIO/ZnTPP was at least ten times larger than that of polyXIO alone at very small applied voltages (less than 1 V). In this case it would appear that the dark current is mainly associated with the presence of ZnTPP. In other words the major contribution to the dark current at

small applied voltages originated from the dye . By the investigation of dark and photovoltaic properties of doped tetraphenylporphyrin sandwich cells, Chamberlain and Coworkers found that the energy between the ground state of the dye and that of a $D^{+}A^{-}$ complex(the dye films were doped with I_2 and O_2-H_2O) was approximately 1.6 eV, which is roughly in agreement with the activation energy (ΔE = 1.5 eV) obtained from the temperature dependence of the dark conductivity measurements[80-84]. ΔE = 1.5 eV in our system does correspond to the energy difference between the ground state of the dye and the redox potential of the pyridine groups of the ion-exchange polymer. It is interesting to note that electron transfer from ZnTPP to pyridine has been observed in solution[15]. This donor-acceptor pair would appear to be responsible for the ΔE of 1.5 eV observed in this system.

3.2 PHOTOCONDUCTIVITY

In order to gain further insight into the charge transport processes in the solid phase, photocurrent measurements were made on the solid state cell with ion-exchange polymer blend films containing ZnTPP. It has been shown previously with the study of photoelectrochemical cells [17,21], that ZnTPP

satisfies the energetic requirements for photoinduced charge separation when incorporated in polyXIO, We therefore chose ZnTPP because this dye was able to produce easily measurable photocurrents in the ion-exchange polymer solid state films. All measurements were done using the experimental setup described in chapter 2. The molecular structure of ZnTPP was shown in Figure 1.3.

3.2.1 SOLID STATE PHOTOCONDUCTIVITY

A large amount of the published data on photoconduction in polymers refers to sensitized or doped materials. In our system the dye, ZnTPP, was added to a host polymer (PolyXIO). Experimentally, the spectral range of sensitivity is extended to longer wavelengths by this technique because there is no significant absorption in the visible region for the polyXIO alone. The net effect of doping is to enable photocurrent response to illumination in the visible spectrum as shown in Figure 3.7. Figure 3.7 Shows the absorption and action spectrum for the SnO_2 OTE/ZnTPP-polyXIO/Au dry cell.

Small photocurrents were observed (about 10^{-10} A) with an action spectrum corresponding to the absorption spectrum of the dye when the SnO_2 OTE/ZnTPP-polyXIO/Au cell described

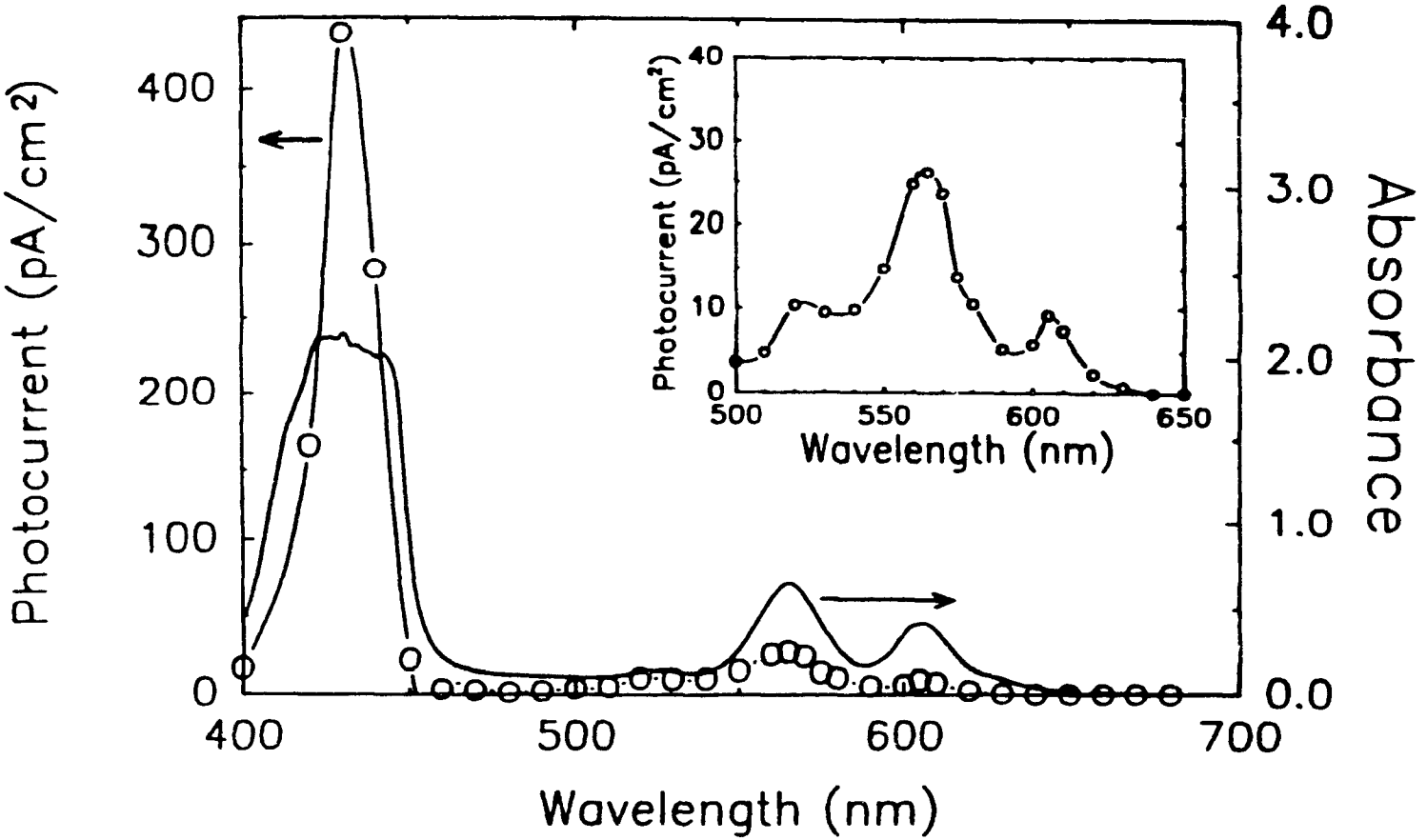

FIGURE 3.7 The action spectrum is shown here along with the absorption spectrum for the Au/ZnTPP-polyXIO/SnO_2 OTE system. The insert gives a closer look at the photocurrents obtained from the absorption by ZnTPP at longer wavelengths(500 to 650 nm)

in chapter 2, was illuminated through the SnO_2. The inset in this figure gives a closer look at the photocurrent in the 500 to 650 nm range. It is obvious that the photocurrent obtained is due to the absorption of light by the dye. The polymer blend film alone shows no significant absorption in the visible region.

3.2.2 THE ISOTHERMAL TIME-DEPENDENCE OF PHOTOCURRENT DECAY

The typical photocurrent decay vs. time for the ZnTPP/polyXIO system is shown in Figure 3.8, after steady state photocurrent was attained under illumination at 606 nm. The inset in the figure shows the complete photocurrent response profile obtained during the light on-light off sequence. The photocurrent-time responses are parallel to those obtained for wet cells [16]. The time constants for dry and wet cells are not experimentally distinguishable. Clearly the time constants refer to charge-transport processes in the solid phase.

Photocurrent responses were measured at different temperatures (22 °C to 42 °C) and at different voltages (0.2V to 0.75V). The experiments were carried out on a number of doped polymer films cast in the same way. The reproducibility of isothermal decay currents was good.

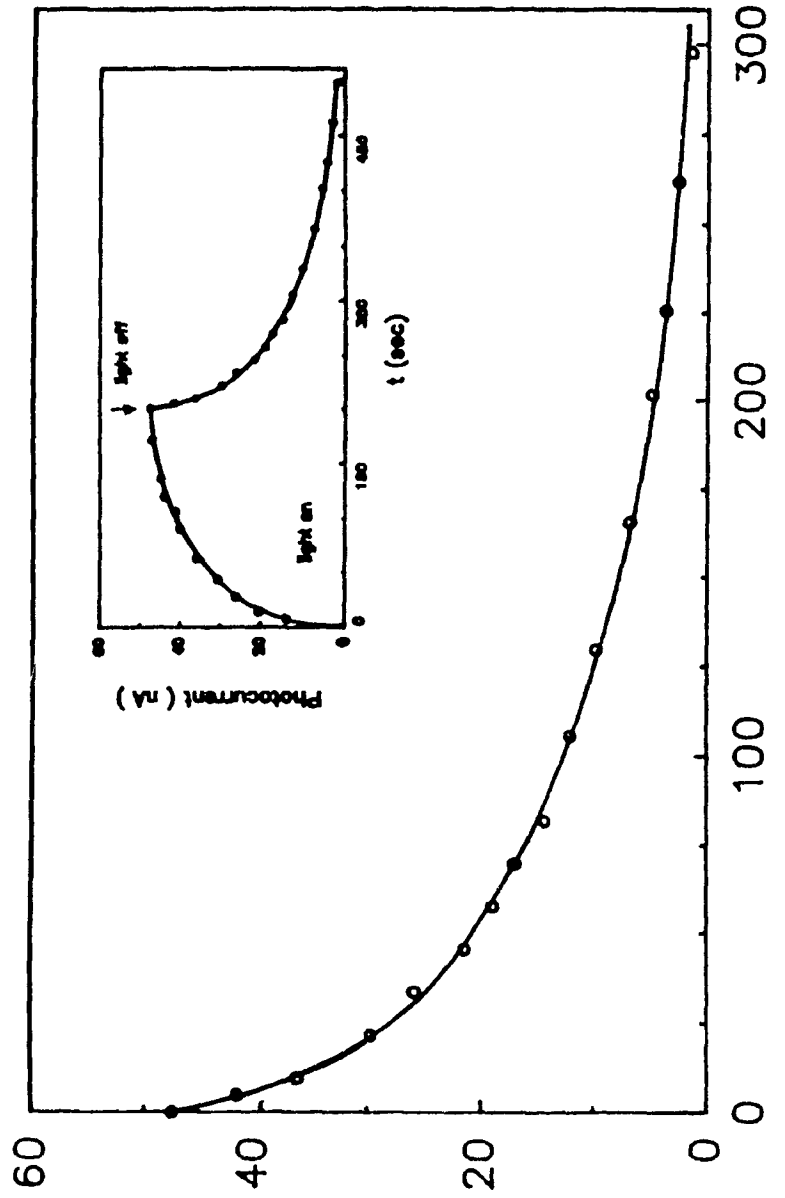

FIGURE 3.8 Photocurrent decay vs. time for the Au/ZnTPP-polyXIO/SnO_2 after steady state photocurrent was attained under illumination at 606 nm(100 $\mu W/cm^2$). Insert shows the complete photocurrent response/profile obtained during the light on- light off sequence.

ZnTPP presents three absorption peaks which are at 606 nm, 566 nm and 430 nm, as shown in the absorption spectrum (Figure 3.7). The isothermal decay currents changed accordingly, that is the shorter the wavelength, the larger the steady state photocurrent and also the longer the time for decay. All photocurrent response profiles were measured at 606 nm because the photon energy at this wavelength (2.1 eV) corresponds to the energy gap between the ground state and lowest excited singlet state of the dye, ZnTPP. Morever, another important reason is the need to generate charges uniformly throughout the bulk of the film rather than at the surface in order to investigate the bulk properties of the ZnTPP/polyXIO system.

All photocurrent decays for the ZnTPP/polyXIO system have long tails. The decay times, however, were found to diminish as the applied voltage or the temperature were raised. Figure 3.9 shows the photocurrent decays vs. time at various temperatures for the system. Similar behaviors were observed for variations of applied voltage. We can account for these phenomena by considering the traps present in these films. We have also seen from the photocurrent decays of the system at short times (first few seconds after the light is turned off) that the photocurrents decay very rapidly, and that at longer times, photocurrent decays slowly until it stabilized. The rapid photocurrent decay in the first few seconds is mainly due to the recombination of

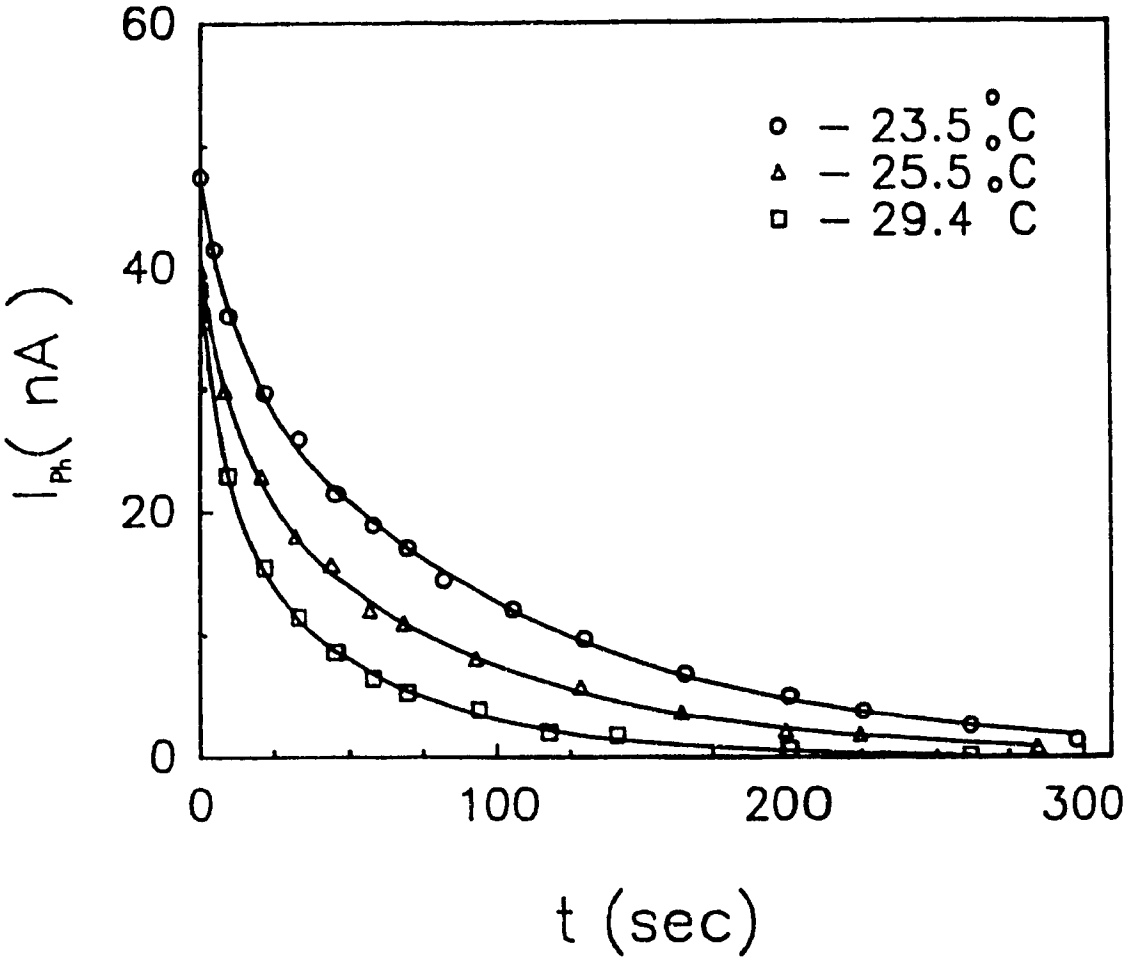

FIGURE 3.9 Photocurrent decays vs. time at various temperatures for Au/ZnTPP-polyXIO/SnO_2 after steady state photocurrent was attained under illumination at 606 nm. (The applied voltage is 0.6V.)

photogenerated charges. These response times (about 1 or 2 seconds) were very short compared to the detrapping response time (about 100 seconds). As will be demonstrated in the following section, the slow detrapping rate is related to the trap depth (0.8 eV) and the average time spent by electrons in the traps.

3.2.3 TEMPERATURE EFFECT

The steady-state photocurrent, under 606 nm illumination, increases with the temperature. Usually this growth is given by the equation[25]:

$$I_{ph} = A \exp\left(-\frac{\Delta E_{ph}}{k\,T}\right) \qquad (3.11)$$

where I_{ph} is the photocurrent, ΔE_{ph} is the thermal activation energy of photoconductance, k is boltzmann's constant, and A is the preexponential constant. Therefore, a plot of ln I_{ph} vs. 1/T will give a straight line (see Figure 3.10). Its slope yields the thermal activation energy of photoconductance ΔE_{ph} which was found to be 0.4 eV. This activation energy does not correspond to ΔE_{therm} of 1.50 eV determined from dark conductance measurements. This is

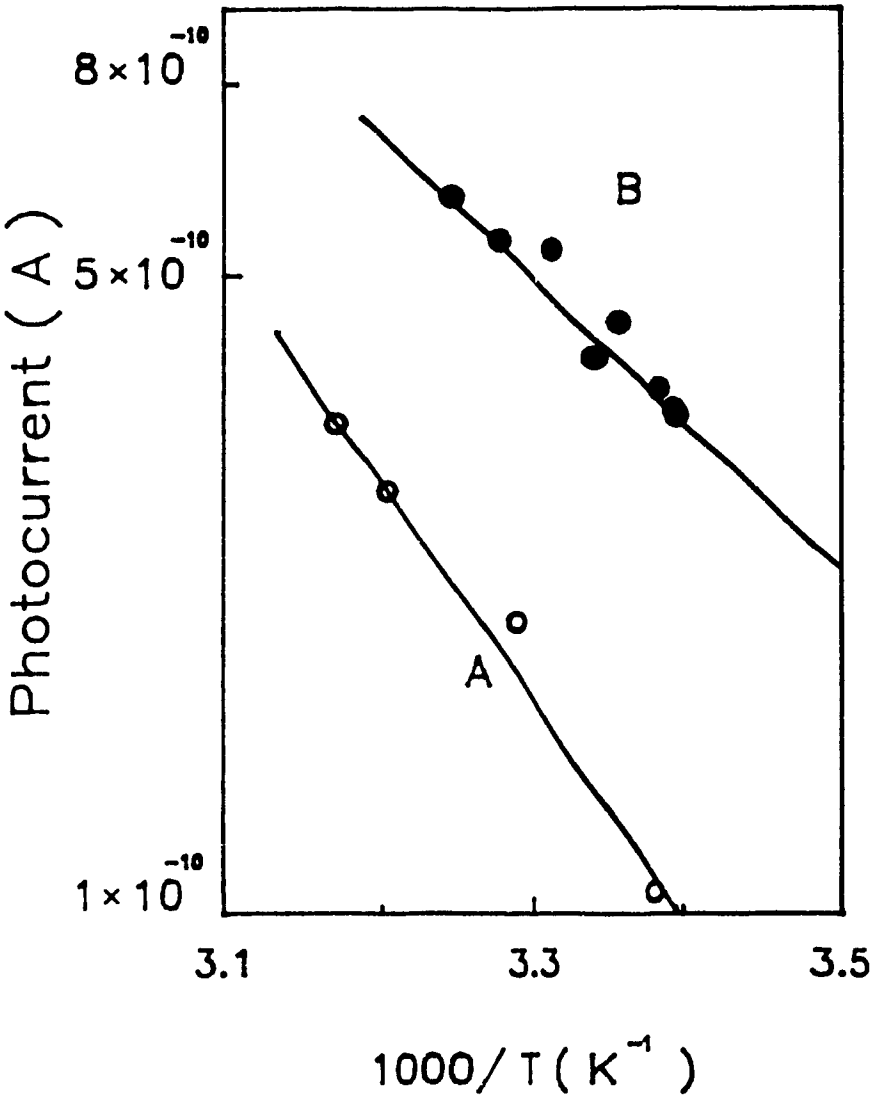

FIGURE 3.10 Dependence of photocurrent on temperature for Au/ZnTPP-polyXIO/SnO_2 system

consistent with values reported in the literature for some other chromophores. For example, values of ΔE_{ph} = 0.44 eV and ΔE_{therm} = 1.5 eV have been reported for orthochrome [25]. For a fluoron derivative, the values ΔE_{ph} (0.25 eV) and ΔE_{therm} (2.0 eV) have also been reported[85].

3.2.4 TRAP PARAMETERS IN THE POLYMER BLEND

When the electrons in a solid with traps are excited, and the excitation source is then removed, the current at constant temperature I_{ph} decreases monotonically with time t. This was illustrated in Figure 3.8 which shows the exponential decay of the photocurrent upon cessation of illumination. It has been shown that when the high field isothermal data are plotted in the form of an It-vs-$\log_{10}$t characteristic (IDC - time vs. Log_{10} time) the shape of the characteristic then provides a direct image of the trap distribution and information on some additional trap parameters[54,55,65].

Isothermal time-dependent current characteristics can be obtained for insulators and semiconductors containing arbitrary trap distributions providing that the applied field is sufficiently high, and that the active region in which the free carriers are generated, is sufficiently thin. Under these conditions, the free carriers are removed from

the active region with negligible recombination.

The measurements of isothermal decay currents in this study were made at applied fields varying from 400 V cm^{-1} to 1500 V cm^{-1}, and the high field data were plotted in the form of an It-vs-$\log_{10}t$ characteristic. Figure 3.11 shows the typical It vs. $\log_{10}t$ characteristics of the SnO_2 OTE/ZnTPP-polyX1O/Au system at various temperatures. These plots appear as asymmetrical bell shaped curves. The $\log_{10}t$ scale can be converted to an energy scale (Figure 3.12) using the following equation:

$$E_c - E_m = kT\ln(\nu t) \qquad (3.12)$$

where E_c is the energy of the conduction band edge, E_m is the energy at the maximum, k is boltzmann's constant, T is the temperature and ν is the attempt-to-escape frequency of electrons in the traps which is usually of the order of 10^{11} to 10^{14} sec^{-1}[54].

A knowledge of the attempt-to-escape frequency is necessary in order to analyze the data. In other words the trap depth can be calculated from the determined attempt-to-escape frequency. This parameter may be determined from experimental data as follows: Let the It-$\log_{10}t$ characteristic be measured at two different temperatures, say, T_1 and T_2. Then one measures the time

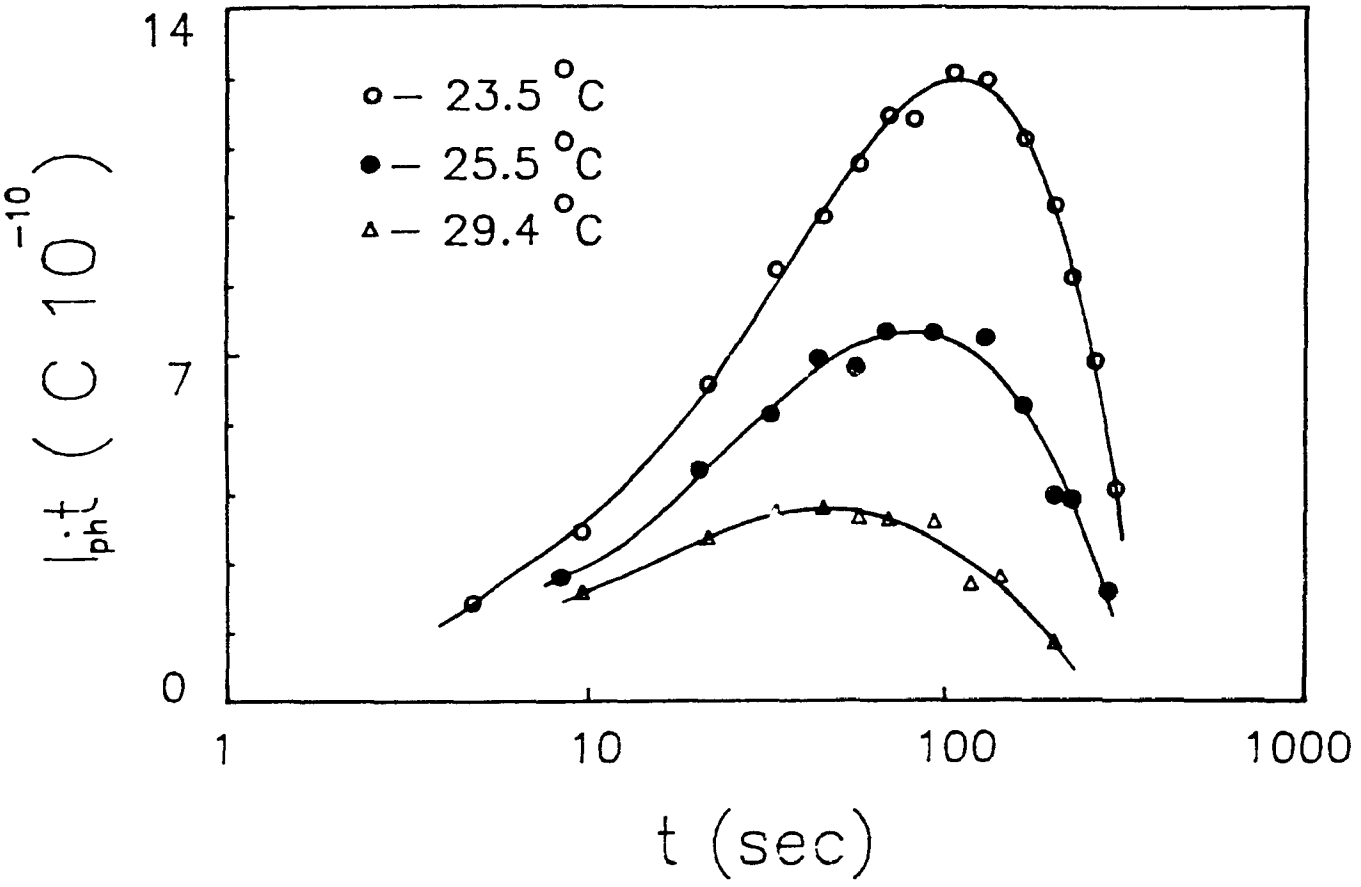

FIGURE 3.11 I-t characteristics of the Au/ZnTPP-polyXIO/SnO_2 system in FIGURE 3.9 were replotted as It vs. $\log_{10}$ t

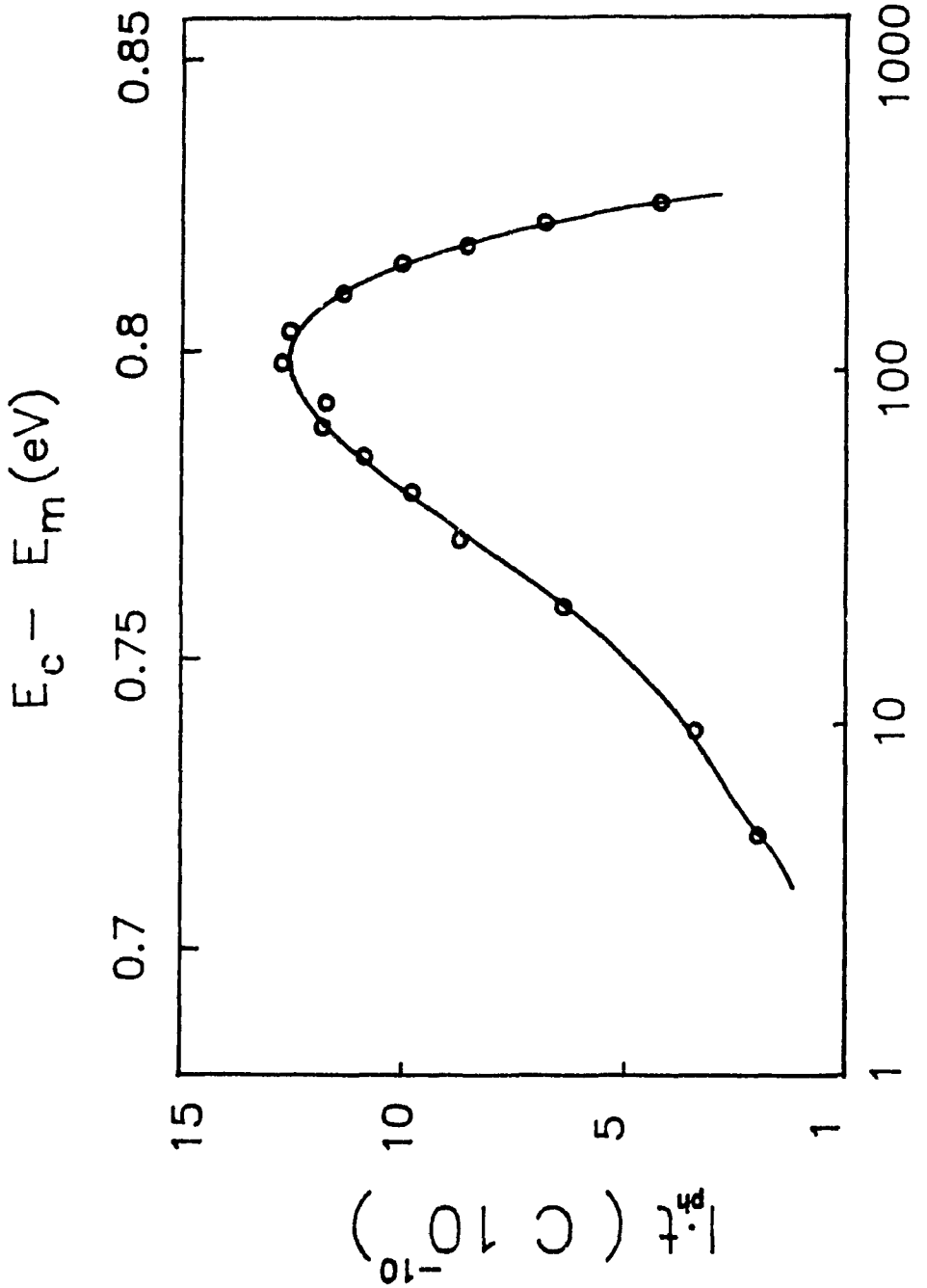

FIGURE 3.12 It vs. $\log_{10}t$ characteristic of ZnTPP/polyXIO system.

t_1 on the $I(T_1)t\text{-}\log_{10}t$, characteristic and t_2 on the $I(T_2)t\text{-}\log_{10}t$ characteristic respectively, t_1 and t_2 being the times at which some prominent part of the characteristic appears corresponding to an energy, say, E_1. Hence, it is then apparent that T_1, T_2, t_1 and t_2 satisfy the following simultaneous equations:

$$E_1 = E_c - kT_1\ln(\nu t_1) \quad , \quad E_1 = E_c - kT_2\ln(\nu t_2) \qquad (3.13)$$

From which ν can be determined by

$$\nu = \exp\left(\frac{T_2\ln(t_2) - T_1\ln(t_1)}{T_1 - T_2} \right) \qquad (3.14)$$

The results for the calculated attempt-to-escape frequencies and trap depths are given in Table 3.5. These values of ν are in good agreement with literature values[54].

We can see from Figure 3.12 that the traps in the ZnTPP/polyXIO system are distributed in a very narrow energy range of about 0.1 eV at a distance ΔE of 0.81 eV from the bottom of the conduction band. If the band gap is much larger compared to the half width of the trap distribution,

it is a good approximation to consider the distribution as a monoenergetic trap level. In light of the measurements described above, we can in principle attribute the peaks obtained from the It-vs-$\log_{10}$t characteristics to a particular trap and determine its depth and attempt-to-escape frequency.

TABLE 3.5

THE ATTEMPT-TO-ESCAPE FREQUENCY (ν) AND THE TRAP DEPTH (ΔE)

Applied Voltages(V)	ν (sec^{-1})	ΔE (eV)
0.2	$7.2 \cdot 10^{11}$	0.82
0.4	$1.9 \cdot 10^{11}$	0.80
0.6	$5.5\ 10^{11}$	0.81
Average	$3.7 \cdot 10^{11}$	0.81

3.2.5 POLYMER / POLYMER CONTACTS

The molecular ion state model has been adopted to account for the observed electron transport process. The energetic distribution of states associated with the hydrophobic domains of the ion-exchange polymer blend used in this study has been evaluated with use of data given in the literature. The experimental and theoretical characterization of the donor and acceptor states for atactic (solution cast) films of polystyrene and poly(2-vinylpyridine) has been reported in detail by Duke and co-workers[33-36]. In addition, they have demonstrated that the distribution of molecular ion states of homopolymers is given by

$$\rho(E) = \rho_A(E) + \rho_D(E) \qquad (3.15)$$

where $\rho_A(E)$ and $\rho_D(E)$ are the densities of molecular ion acceptor states and donors states, respectively. They have also determined that the molecular ion states of a copolymer(a mixture of two homopolymers) may be taken as the simple linear superposition of the different component state distributions:

$$\rho(E) = \kappa\ \rho_1(E) + (1 - \kappa)\ \rho_2(E) \qquad (3.16)$$

where κ is the mole-fraction of component 1 in the

copolymer(or mixture), E is the insulator charge state energy and ρ_i describes the double-Gaussian-state density of the component i in the copolymer(or mixture). We have employed Eq. 3.12 for our purposes by assuming that the hydrophobic domains in the ion-exchange polymer were composed of 0.4 and 0.6 in molar fractions of polystyrene and poly(4-vinylpyridine), respectively. These are the molar fractions of each component that are added at the outset, when the mixture is prepared. The resulting distribution is shown in Figure 3.13 which presents an energy level diagram combining all constituents of the system under consideration. The donor and acceptor state densities have been normalized to correspond to the maximum density of states, about 4 10^{15} cm^{-3} involved in the contact charge exchange experiments according to Duke and Fabish[35].

The donor and acceptor state distributions appearing in Figure 3.13 are approximate, because of the assumption that the hydrophobic domains present in the cast films contain the same molar fractions of polystyrene and poly (4-vinylpyridine) as that used in preparing the polymer blend previous to casting. In addition the literature data used for the calculation related to poly(2-vinyl- pyridine). The energetic distribution of molecular ion states for atactic poly(4-vinylpyridine) have yet to be established experimentally or theoretically. Nevertheless, the location of the distribution centroid <E> which is a deciding factor

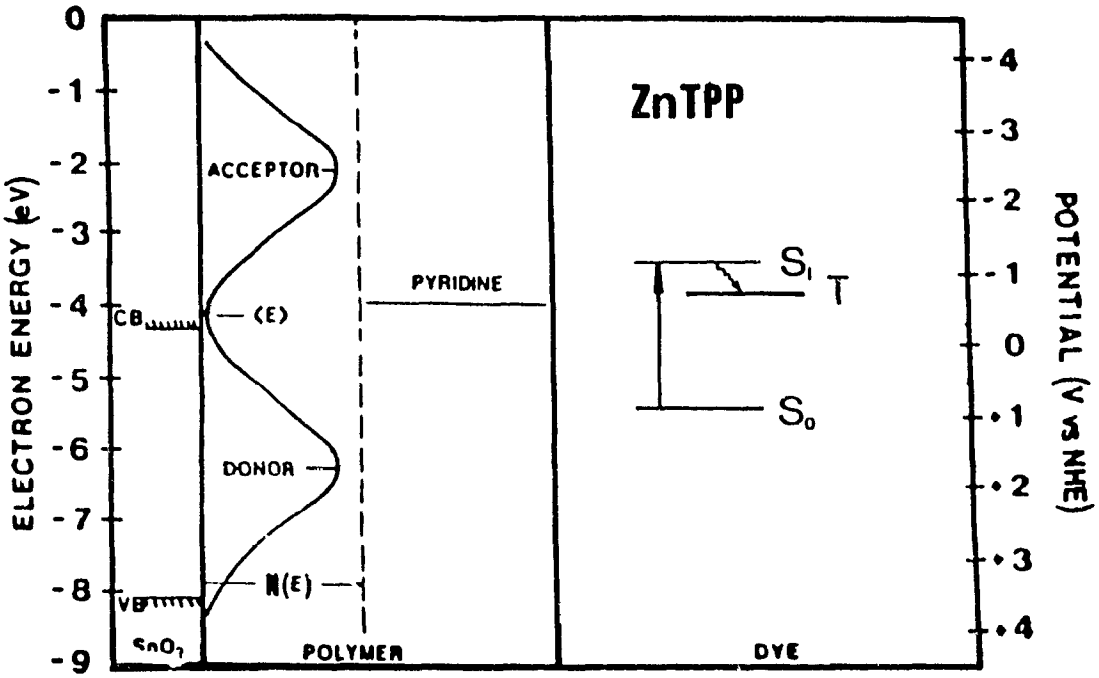

FIGURE 3.13 Energy level diagram. The calculated distribution of acceptor and donor states of the polymer blend is shown here relative to the energy levels of the SnO_2 OTE, the pyridne redox potential, and the ZnTPP dye used in the studies.

as to whether or not acceptor levels are available for the conduction electrons injected by the excited dyes, is not expected to move significantly toward higher energies because of a difference in polymer composition or a change in the nitrogen's position within the pyridine group [17]. From the dark conductivity measurements the energy gap or the distance between the centroids <E>, was found to be 4.0 eV which is in agreement with the gap predicted in the energy diagram of Figure 3.13, The quaternized groups of the ion-exchange polymer blend, which have been shown to make up the outer surfaces of the hydrophobic domains in the film (separating the hydrophobic domains by hydrophilic domains[2,3,5]) were not taken into account in the model. At the moment, the effect of these pendant groups on the distributions of molecular ion-state is not clear. However, the energy relationship between the different components of the system would seem to account for the photoinduced charge-separation process. The low activation energy for photoconductance of ΔE_{ph} = 0.4 eV may be related to the transfer of photogenerated charges between hydrophobic domains (through hydrophilic regions).

The ground- and excited-state energy levels of the dye (ZnTPP) are shown in Figure 3.13 where they are compared with the redox potential of the pyridine groups in the polymer. The acceptor states forming the upper half of the distribution are believed to transport the photogenerated

charges transferred to the polymer, all the way to the SnO_2 OTE. It is worth noting that the contact charge experiments performed by Fabish et al. demonstrated that the injection of electrons in pendant group polymers typically extended to distances of 4μm, and the thickness of the ZnTPP/polyXIO films we used is about 5 μm.

The valence and conduction band positions of the SnO_2 are indicated on the left-hand side of Figure 3.13. Because of the degeneracy, the Fermi level of the highly conducting SnO_2 coincides with its conduction band. The first excited-state levels of ZnTPP are located at energies which favor electron transfer to the polymer. The excited singlet and triplet state of ZnTPP are situated at energies of -3.43 eV and -3.90 eV, respectively. The shape and energy parameters of the trap distribution shown in Figure 3.12, however, differ from the molecular ion state distributions which were calculated from Eq.3.16, under the assumption that the styrene and pyridine groups of the polyXIO were homogeneously distributed in the hydrophobic regions. The results shown in Figure 3.12 may provide evidence for the existence of a distribution of charge-transfer states which results when two different polymers come into contact. Duke and Fabish have also demonstrated that the charge injection mechanism observed for metal/polymer contact charge exchange also applies to polymer/polymer contacts and , therefore, they concluded that charge exchange between two polymers

will occur at all energies for which filled donor states of one polymer overlap with empty acceptor states of the other[35,36].

This is more clearly illustrated in Figure 3.14. The charge-transfer integrand resulting from the overlap of acceptor states of insulator 1 (PS, polystyrene) with the donor states of insulator 2 (PVP, polyvinylpyridine) is bounded by their distribution centroids $< E_1 >$ and $< E_2 >$. The charge transfer integrand (CTI) shown in Figure 3.14 was calculated in the region between -4.8 eV ($<E_1>$) and -3.4 eV ($<E_2>$) from the equation:

$$CTI = \int \min \left[\rho_A^{PS} \rho_D^{PVP} \right] f_2(E) \left[1 - f_1(E) \right] \qquad (3.17)$$

where ρ is the density of acceptor (A) or donor (D) states for PS or PVP, $\min \left[\rho_A^{PS} \rho_D^{PVP}\right]$ is the lesser of the two densities at energy E, $f_2(E)$ is the probability of the donor states of PVP being occupied and $\left[1-f_1(E)\right]$ is the probability of acceptor states of PS being empty. Molecular ion state data was obtained from the literature for PS and PVP [74,75]. The state occupation probability, f(E), is

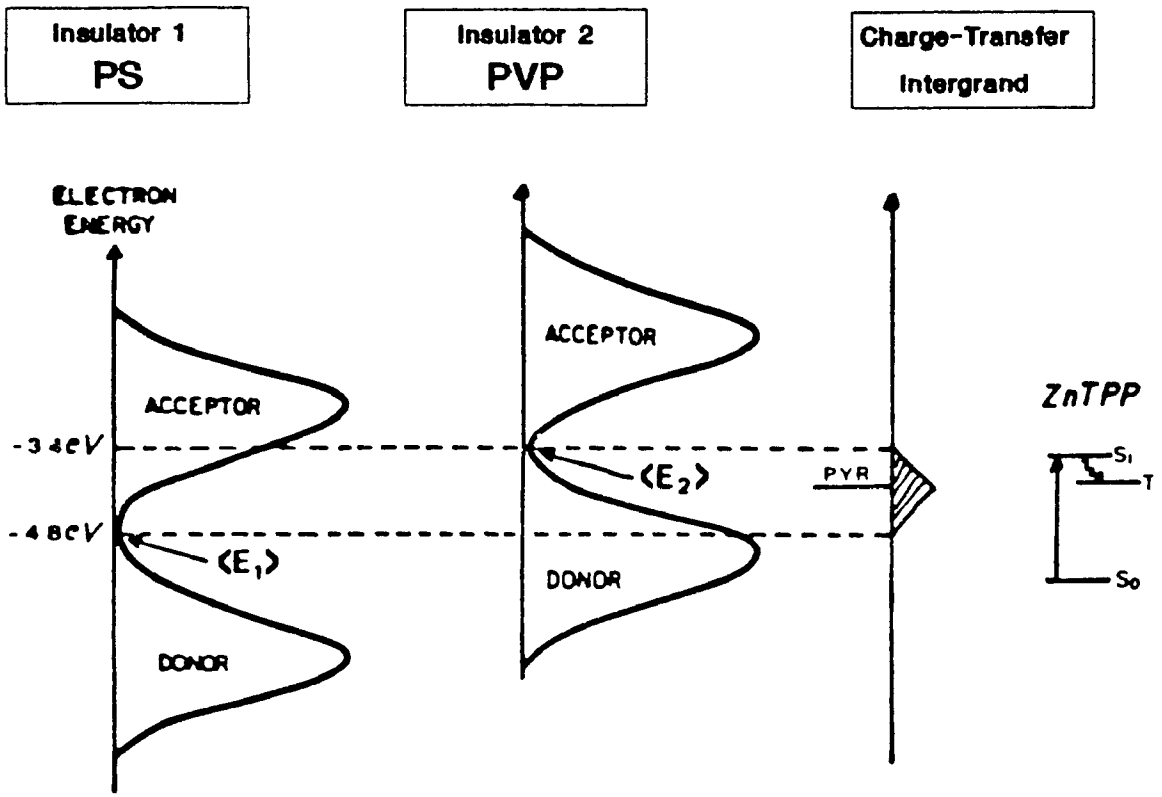

FIGURE 3.14 Schematic illustration of the dominating charge transfer states in polymer/polymer (PS/PVP) contact associated the dye ZnTPP

$$f(E) = \frac{1}{e^{(E - \langle E \rangle)/kT} + 1} \qquad (3.18)$$

in the same region bounded by $\langle E_1 \rangle$ and $\langle E_2 \rangle$ shown in Figure 3.14.

The experimentally obtained trap state distribution shown in Figure 4.6 has its maximum at an energy very close to the charge-transfer integrand maximum shown in Figure 3.14, if the conduction band energy, E_c, is taken to be the first existed singlet-state energy level of the ZnTPP dye. The concentration of ZnTPP, N_{ZnTPP} in the film is about $2.5 \cdot 10^{20}$ molecules/cm^3. If one uses following equation

$$R_{ZnTPP} = \left(\frac{3}{4 \pi N_{ZnTPP}} \right)^{1/3} \qquad (3.19)$$

to estimate an average radius, R_{ZnTPP}, by considering each ZnTPP molecule as a sphere, one gets the radius about 10 Å. This average distance is very close to the size of the dye molecules, which means that they are close enough to interact, in other words, to form a band. Also included in Figure 3.13 are the redox energy levels of the ZnTPP dye and

the reduction potential for the pyridinium moiety. The calculated charge transfer integrand and experimentally obtained trap state distribution for the polymer blend both have their maximum centered at around the reduction potential for pyridinium groups.

These results indicate that the internal morphology of the hydrophobic regions of the polymer blend may consist of islands of styrene groups in contact with islands of pyridine groups mixed with regions composed of a homogeneous blend of their respective pendant groups.

CHAPTER 4 THE PHOTOCONDUCTIVITY MODEL

(Further Discussion)

In this chapter the simplified photoconductivity model will be used to estimate the lifetime and related parameters of the generated carriers.The advantages of this simplified model are that analytical solutions can be obtained and that we can gain more insight into the charge transport processes.

4.1 INTRODUCTION

In a solid, quantum mechanical considerations and the periodic nature of the potential energy associated with the atomic cores lead to quasi-continuous bands of energy which can be occupied by electrons that are mobile, separated by bands of forbidden energies. Impurities (donors, acceptors, etc.) or crystal defects, however, can and do introduce allowable energy levels in the forbidden gap. It is now known that periodicity is not a necessary requirement to electron mobility and even amorphous materials offer regions where electrons are mobile[19,37].

Photoconductivity is observed in a solid where a radiation source raises an electron from a nonconducting state

(valence band) to a conducting state (conduction band) where it is free to contribute to electrical conductivity. The vacancy caused in the initially filled valence band acts as a free carrier of positive sign (a hole) and can also contribute to electrical conductivity. The free electrons and holes that are thus excited can recombine, ultimately returning the solid to its initial state. The direct recombination of electrons and holes is a very unlikely process for free carrier densities occurring under normal operating conditions. The recombination takes place through the so-called recombination centers introduced in the forbidden energy zone either by defects or by chemical impurities. The recombination itself is a two step process in that one of the carriers is trapped at the recombination center, followed by the trapping of a carrier of opposite charge at the same site. However, before the excitation is terminated by recombination, each type of carrier may be trapped (immobilized) and released (freed) at the trapping centers. A recombination center is a site where the captured carrier has a greater probability of combining with a carrier of opposite sign than of getting thermally excited into its free state, whereas the trapping center is a site where a trapped carrier has a greater probability of being thermally excited into its free state than that of uniting with a carrier of the opposite sign[86-90].

4.2 TRAPPING EFFECTS

A continuous distribution of traps was shown in Figure 4.5 and Figure 4.6 to be present in the ZnTPP/PolyIXO system. However. it was obvious that the width of the distribution was very narrow (less than 0.1 eV) compared with the band gap of ZnTPP (about 2 eV).It is a good assumption then, that the trap distribution be considered as a single set of discrete trapping levels for electrons approximately located at a distance E_{max} of about 0.8 eV below the bottom of the conduction band, as shown in Figure 4.1.

Consider now the free-electron density in the simple model shown in Figure 4.1. In this case we consider an insulator, such as a doped polymer, in which f carrier pairs are being generated per second by absorbed radiation. n/τ is the rate at which a set of recombination centers empties out electrons from the band. In addition, we assume a set of N_t trapping states per unit volume, of which n_t are occupied by electrons. The transition probability from the conduction band to the trap is denoted C_{nt}, so that the trapping rate r_{nt} is given by the product of this probability and the density of states involved in the transition, *i.e.*,

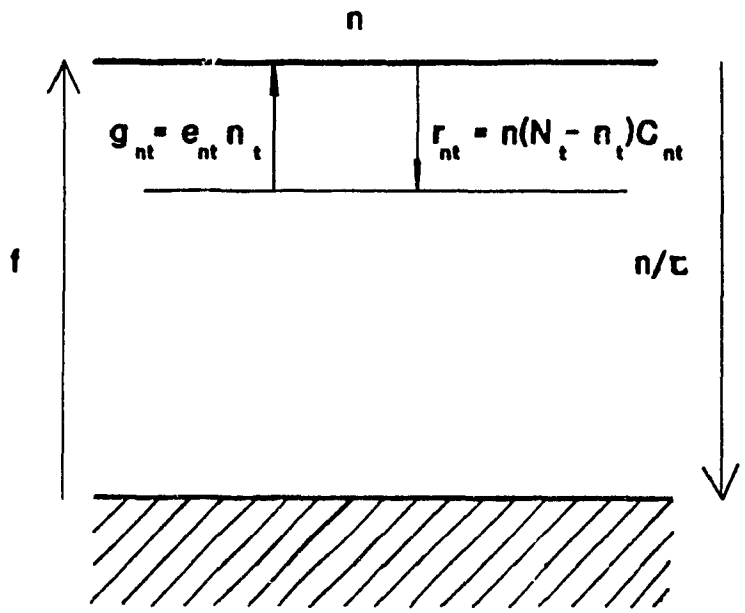

FIGURE 4.1 Single set of trapping levels for electrons

$$r_{nt} = n(N_t - n_t)C_{nt} \qquad (4.1)$$

The thermal generation rate from the traps into the conduction band will be given by the product of the number of trapped electrons, the transition probability to a state in the conduction band, and the density of these final states. The latter two factors are denoted by e_{nt}, so that the generation rate is given by

$$g_{nt} = e_{nt} n_t \qquad (4.2)$$

With this model, we can write the rate equations for the free-and trapped-electron densities as

$$dn/dt = f - (n / \tau) + e_{nt} n_t - n(N_t - n_t)C_{nt} \qquad (4.3a)$$

$$dn_t/dt = -e_{nt} n_t + n(N_t - n_t)C_{nt} \qquad (4.3b)$$

In the steady state, we have

$$n_o = f\tau \quad , \quad n_{to} = f\tau(N_t - n_{to})C_{nt} \qquad (4.4)$$

In order to solve for the decay of the photocurrent, we make the further assumption that we are working under conditions of low illumination levels and high trap density, $N_t \gg n_t$. For the photocurrent decay, the light source has been removed, therefore f = 0. In this case Eqs. 4.3 become

$$dn/dt = - (n / \tau) + e_{nt} n_t - n N_t C_{nt} \qquad (4.5a)$$

$$dn_t/dt = -e_{nt} n_t + n N_t C_{nt} \qquad (4.5b)$$

where $N_t \gg n_t$ has been used. A solution to Eq.4.5a is

$$n = a_1 \exp(-t/\tau_1) + a_2 \exp(-t/\tau_2) \qquad (4.6)$$

where a_1, a_2 are constants of integration, and τ_1 and τ_2 are some algebraic functions of the constants in Eqs 4.5. Substituting Eq. 4.6 into Eq. 4.5b we have

$$dn_t/dt + e_{nt} n_t =$$

$$C_{nt} N_t a_1 \exp(-t/\tau_1) + C_{nt} N_t a_2 \exp(-t/\tau_2) \qquad (4.7)$$

We know the standard formula

$$dy/dt + P(t)y = Q(t) \qquad (4.8)$$

and the solution of this equation is

$$y(t) = e^{-\int P dt} \left[\int Q(t)\ e^{\int P dt}\ dt + C \right] \qquad (4.9)$$

According to Eq.4.9 the solution of Eq.4.7 is

$$n_t = e^{-\int e_{nt} dt} \left[\int C_{nt} N_t \left(a_1 e^{-t/\tau_1} + a_2 e^{-t/\tau_2} \right) e^{\int e_{nt} dt} dt + C \right]$$

$$= \frac{C_{nt} N_t}{e_{nt} - \tau_1^{-1}} a_1 e^{-t/\tau_1} + \frac{C_{nt} N_t}{e_{nt} - \tau_2^{-1}} a_2 e^{-t/\tau_2} + C e^{-e_{nt} t} \qquad (4.10)$$

Now that we know the solutions of n and n_t we can substitute Eq.4.6 and Eq.4.10 into Eq.4.5a in order to determine constants τ_1 and τ_2. So we get

$$\left[\frac{e_{nt} C_{nt} N_t}{e_{nt} - \tau_1^{-1}} - 1/\tau - N_t C_{nt} + 1/\tau_1 \right] a_1 e^{-t/\tau_1} +$$

$$\left[\frac{e_{nt} C_{nt} N_t}{e_{nt} - \tau_2^{-1}} - 1/\tau - N_t C_{nt} + 1/\tau_2 \right] a_2 e^{-t/\tau_2} +$$

$$e_{nt} C \exp(-e_{nt} t) = 0 \qquad (4.11)$$

Because $\exp(-1/\tau_1)$, $\exp(-1/\tau_2)$ and $\exp(-e_{nt} t)$ are linearly independent, it is obvious that

$$C = 0 \qquad (4.12)$$

$$\frac{e_{nt}C_{nt}N_t}{e_{nt} - r} - 1/\tau - N_tC_{nt} + r = 0 \qquad (4.13)$$

where $r = 1/\tau_1$ or $1/\tau_2$. Rearranging Eq.4.13 we have

$$r^2 - (1/\tau + N_tC_{nt} + e_{nt})r + e_{nt}/\tau = 0 \qquad (4.14)$$

The solutions of Eq.4.14 are

$$r_{\pm} = \frac{1}{2}\left[(\frac{1}{\tau} + N_tC_{nt} + e_{nt}) \pm \sqrt{(1/\tau + N_tC_{nt} + e_{nt})^2 - 4e_{nt}/\tau} \right] \qquad (4.15)$$

We should choose linearly independent solutions. So

$$\tau_1 = 1/r_+ \text{ and } \tau_2 = 1/r_- \qquad (4.16)$$

Taking two linearly independent solutions we have

$$n = a_1\exp(-t/\tau_1) + a_2\exp(-t/\tau_2) \qquad (4.17)$$

$$n_t = \frac{C_{nt} N_t}{e_{nt} - \tau_1^{-1}} a_1 e^{-t/\tau_1} + \frac{C_{nt} N_t}{e_{nt} - \tau_2^{-1}} a_2 e^{-t/\tau_2} \qquad (4.18)$$

where $\tau_1 = 1/r_+$ and $\tau_2 = 1/r_-$. The constants, a_1 and a_2, can be found by applying the initial condition for the decay to Eqs.4.5.

at t=0 $n_o = f\tau$, $n_{to} = f\tau N_t C_{nt}/e_{nt}$

With this, we have

$$\begin{cases} f\tau = a_1 + a_2 \\ f\tau \dfrac{N_t C_{nt}}{e_{nt}} = \dfrac{N_t C_{nt}}{e_{nt} - \tau_1^{-1}} a_1 + \dfrac{N_t C_{nt}}{e_{nt} - \tau_2^{-1}} a_2 \end{cases} \qquad (4.19)$$

Solving Eqs.4.19 we have

$$a_1 = f\tau \frac{(1 - \tau_1 e_{nt})}{(\tau_2 - \tau_1) e_{nt}} \quad , \quad a_2 = f\tau \frac{(\tau_2 e_{nt} - 1)}{(\tau_2 - \tau_1) e_{nt}} \qquad (4.20)$$

If we take $a_1/a_2 = a$ and rearrange Eq. 4.20 we find

$$e_{nt} = \frac{1 + a}{\tau_2 a + \tau_1} \qquad (4.21)$$

From Eqs.4.15 and 4.16 we known that

$$1/\tau_1 = r_+ = \frac{1}{2}\left[(1/\tau + N_t C_{nt} + e_{nt}) + \sqrt{(1/\tau + N_t C_{nt} + e_{nt})^2 - 4e_{nt}/\tau} \right] \qquad (4.22)$$

$$1/\tau_2 = r_- = \frac{1}{2}\left[(1/\tau + N_t C_{nt} + e_{nt}) - \sqrt{(1/\tau + N_t C_{nt} + e_{nt})^2 - 4e_{nt}/\tau} \right] \qquad (4.23)$$

Rearranging Eqs.4.22 and 4.23 gives

$$y + z + e_{nt} + \sqrt{(y + z + e_{nt})^2 - 4e_{nt}y} = 2/\tau_1 \qquad (4.24a)$$

$$y + z + e_{nt} - \sqrt{(y + z + e_{nt})^2 - 4e_{nt}y} = 2/\tau_2 \qquad (4.24b)$$

where $y = 1/\tau$ and $z = N_t C_{nt}$ have been used. If we add Eq.4.24a and Eq.4.24b we have

$$y + z + e_{nt} = 1/\tau_1 + 1/\tau_2 \qquad (4.25)$$

Similarly, subtracting Eq.4.24b from Eq.4.24a we get

$$\sqrt{(y + z + e_{nt})^2 - 4e_{nt}y} = 1/\tau_1 - 1/\tau_2 \qquad (4.26)$$

Rearranging Eq.4.26 we have

$$y = \frac{1}{4e_{nt}} \left[(y + z + e_{nt})^2 - (1/\tau_1 - 1/\tau_2)^2 \right] \qquad (4.27)$$

Substituting Eq.4.25 into Eq.4.27 we get

$$y = 1/(e_{nt}\tau_1\tau_2) \qquad (4.28)$$

From Eq.4.25 we have

$$z = (1/\tau_1 + 1/\tau_2) - y - e_{nt} \qquad (4.29)$$

Finally we get

$$\tau = e_{nt}\tau_1\tau_2 \qquad (4.30)$$

$$N_t C_{nt} = (1/\tau_1 + 1/\tau_2) - 1/\tau - e_{nt} \qquad (4.31)$$

The solutions are summarized in the following:

$$n = a_1 \exp(-t/\tau_1) + a_2 \exp(-t/\tau_2)$$

$$n_t = \frac{C_{nt} N_t}{e_{nt} - \tau_1^{-1}} a_1 e^{-t/\tau_1} + \frac{C_{nt} N_t}{e_{nt} - \tau_2^{-1}} a_2 e^{-t/\tau_2} \tag{4.32}$$

where constants a_1 , a_2, τ, and $C_{nt} N_t$ are:

$$a_1 = f\tau \frac{(1 - \tau_1 e_{nt})}{(\tau_2 - \tau_1)\, e_{nt}} \quad , \quad a_2 = f\tau \frac{(\tau_2 e_{nt} - 1)}{(\tau_2 - \tau_1)\, e_{nt}} \tag{4.33}$$

$$e_{nt} = \frac{1 + a}{\tau_2 a + \tau_1} \quad ; \qquad \tau = e_{nt} \tau_1 \tau_2$$

$$N_t C_{nt} = (1/\tau_1 + 1/\tau_2) - 1/\tau - e_{nt} \tag{4.34}$$

If we assume that the condition $N_t C_{nt} \gg 1/\tau$ applies, which means that the thermally generated traffic between the trapping states and the conduction band is much more rapid than the recombination process by which electrons are removed from the conduction band(we will see in the following section that this is in fact not the case), Eqs.4.22 and 4.23 can be simplified to

$$\tau_1 = \frac{\tau}{1 + N_t C_{nt} \tau} \quad ; \quad \tau_2 = \frac{1 + N_t C_{nt} \tau}{e_{nt}} \qquad (4.35)$$

and Eq.4.33 becomes

$$a_1 = \frac{1}{1 + N_t C_{nt} \tau} f\tau \quad ; a_2 = \frac{N_t C_{nt} \tau}{1 + N_t C_{nt} \tau} f\tau \qquad (4.36)$$

Eqs.4.35 and 4.36 are the same expressions as those described by Sadasiv. [90].

4.3 ANALYSIS OF RESULTS

The photocurrent decay characteristics for the Au/ZnTPP-polyXIO/ SnO_2 system shown in Chapter 3 can be approximately expressed in the following form

$$I_{ph} = A_1 \exp(-t/\tau_1) + A_2 \exp(-t/\tau_2) \qquad (4.37)$$

for the decay because the current is proportional to the concentration of free electrons. The concentration of free electrons should have the same characteristic time constant and the same ratios for the coefficients. The response time constants τ_1 and τ_2 and the ratio a_1/a_2 can therefore be found from photocurrent decay curves. To do so, the best fit

to the photocurrent decay curve is obtained, as shown in Figure 4.2. This yields the following parameters

$\tau_1 = 131$ sec; $\tau_2 = 10.8$ sec

$a_1/a_2 = A_1/A_2 = 2.0$ at 23.2 °C

From Eq.4.34 we have $e_{nt} = 0.02\ sec^{-1}$, $\tau = 26$ sec and $C_{nt}N_t = 0.05\ sec^{-1}$. The ratio of the free electrons to the trapped electrons can be obtained if the first few seconds of this decay curve are omitted. The second terms for both n and n_t (Eq. 4.32) become negligible after the first few seconds because $\tau_1 \gg \tau_2$. So for most of the decay, the ratio, n/n_t, can be taken as the ratio of the first terms. Then we have

$$\frac{n}{n_t} = \frac{e_{nt} - \tau_1^{-1}}{C_{nt}N_t} \qquad (4.38)$$

The results thus obtained are summarized in Table 4.1. The calculated results are consistent with the previous assumption that e_{nt} is small. The long response times (τ_1) indicate the slowness of the detrapping process which is related to the deep trap depth (about 0.8 eV). In this model we are unable to calculate the average time spent by the electrons in the traps. The short response times(τ_2) is mainly due to recombination. From the response times or lifetimes, a variation similar to the one shown in Figure 3.9 at various temperatures is observed. As the temperature rises the lifetime decreases.

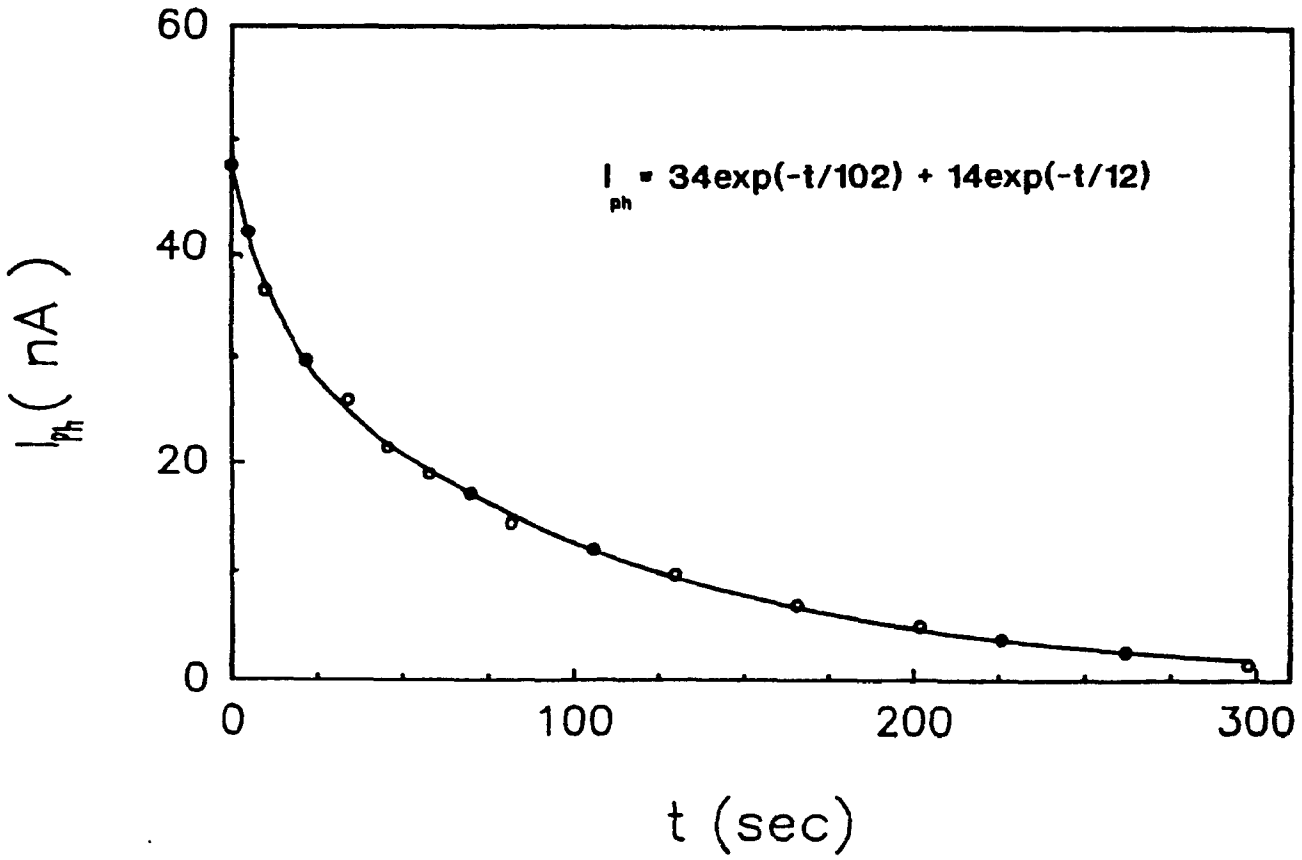

FIGURE 4.2 The experimental data(open circles) was fitted with a double exponential equation(solid line) derived from the photoconductivity model

By rewriting Eq.4.3a as following

$$\frac{dn}{dt} = - n \left(- \frac{1}{\tau} + e_{nt} \frac{n_t}{n} - N_t C_{nt} \right) \qquad (4.38)$$

we can make a comparison between the relative recombination rate ($1/\tau$), the relative detrapping rate ($e_{nt} n_t/n$) and the relative retrapping rate($N_t C_{nt}$). These relative rates were calculated from Table 4.1 and are listed in Table 4.2. We can see that the relative recombination rates and the relative retrapping rates are approximately the same. The relative thermal excitation rates are two times larger but not large enough to consider that the other two rates are negligible (as was assumed previously in Chapter 3). This problem is mainly because we can not take data from the photocurrent decay curves as precisely as needed, especially at the very first few seconds. There is a large drop of the photocurrent just after the light is turned off. So the shorter response times obtained from the fitted curves are much larger than they should be. All calculated parameters are based on the responses times and the ratio of the two preexponential factors. This problem can be solved by connecting the electrometer directly to a computer rather than a recorder. It is also noteworthy, that we are not dealing with a monoenergetic set of trapping states. the traps are slightly distributed (about 0.1 eV).

TABLE 4.1

Photocurrent decay data for the ZnTPP/polyXIO cell

Temperature	23.2 ^{o}C	26.2 ^{o}C	30.8 ^{o}C
Response time τ_1(sec)	131	126	91
Response time τ_2(sec)	10	9	7
a_1/a_2	2.0	1.9	1.8
e_{nt} (sec^{-1})	0.02	0.02	0.03
Life time τ (sec)	26	23	17
n/n_t	0.2	0.2	0.2
$C_{nt}N_t$ (sec^{-1})	0.05	0.06	0.07

Table 4.2

Calculated data for the ZnTPP/polyXIO cell

from the photoconductivity model

T(°C)	$1/\tau$ (sec^{-1})	$N_t C_{nt}$ (sec^{-1})	$e_{nt} n_t/n$ (sec^{-1})
23.2	0.04	0.05	0.08
26.2	0.04	0.06	0.09
30.8	0.05	0.07	0.12

Chapter 5
Conclusion and Outlook

The effort to explore the electrical and related properties of ZnTPP incorporated into an ion-exchange polymer blend has been stimulated by their potential application for the conversion and storage of solar energy. The main feature of this type of polymer is its spontaneous tendency to segregate into hydrophilic and hydrophobic domains. It is now believed that the system operates under both ionic and "dry" electronic conduction mechanisms. The comparison with other types of materials like doped semiconductors has yielded new insight into the basic phenomena of charge transport in disordered materials. The results show very good consistency in various ways of investigation and are in good agreement with the literature values.

The system has been proven to be capable of performing the spatial separation of photogenerated charges. The energetic requirements of this dye/polymer model has been established which can be used as a guideline to improve efficiencies in such a system to interesting levels.

References

1. Ikeda, T.; Schmehl, R.; Denisevich, P.; Willman, K.; Murray R. W. J. Am. Chem. Soc. 1982, 104, 2683.

2. Montgomery, D.D.; Anson, F.C. J. Am. Chem. Soc. 1985, 107, 3431.

3. Sumi, K.; Anson, F.C. J. Phys. chem. 1986, 90, 3845.

4. Chidsey, C.E.D.; Murray, R.W. J. Phys. Chem. 1986, 90,1479.

5. Inoue, T.; Anson, F.C. J. phys. Chem. 1987, 91, 1519.

6. Oyama, N. and Anson, F.C.; J. Electrochem. Soc. 127, 247, 1980

7. Oyama, N.; Shimomura, T.; Shigehara, K.; Anson, F.C.; J. Electrochem. 112, 271, 1980

8. Oyama, N.; Anson, F.C. Anal. Chem. 52, 1192, 1980

9. Montgomery, D.D.; Tsuchida, E.; Shigehara, K. and Anson. F.C.; J. Am. Chem. Soc. 106, 7991, 1984

10. Oyama, N.; Shuichiro, Y.; Nishiki, Y.; Tokuda, K.; Matsuda, H. and Anson, F.C.; J. Electroanal. Chem., 139, 371, 1982

11. Ham, G.E., Ed.; "copolymerization"; Wiley-Interscience; New York, 1964

12. Morgan, P.W. "Condensation Polymers: By Interfacial and Solution Methods"; Wiley-Interscience; New York' 1965

13. Sorenson, W.R.; Campbell, T.W."Preparative Methods of

Polymer Chemistry", 2nd ed.; Wiley-Interscience; New York, 1968

14. Crouch, A. M.; Langford, C.H. J. Electroanal. Chem. Interfacil Electrochem. 1987, 221, 83.

15. Crouch, A.M.; Sharma, D.K. and Langford, C.H.; J. Chem. Soc. Chem. Commun., 1988

16 Crouch, A.M.; Ordonez, I.; Langford, C.H. and Lawrence, M.F.J. Phys.Chem. Vol. 92 No21 1988

17. Allcock, H.R.; Polymer and Polymerization; Englewood Cliff. N.J. 1981

18. Seanor, D.A.; Influence of Polymer structure on the electric and Photoelectric Properties of polymers, Ed. Patsis, A.V. and Seanor, D.A., Photoconductivity in Polymers An interdisciplinary Approach; Technomic Co. Inc. 1976

19. Rencroft, P.J.; Photoconduction Mechanisms in Polymeric Solid, Ed. Patsis, A.V. and Seanor, D.A., Photoconductivity in Polymers An interdisciplinary Approach; Technomic Co. Inc. 1976

20. McGlym, S.P.; Azumi, T. and Kinoshita, M.; Molecular Spectroscopy of The triplet State; Prentice-hall, Inc. Englewood Cliff, New Jersey, 1969

21. Ishmael.Ô.D. Ph.D dissertation (Concordia University Montreal, Quebec. 1989).

22. Epstein, A.; and Wildi, B.S.; J. Chem. Phys. 32, 324, 1960

23. Gutmann, F.; and Lyons, L.E.; Organic Semiconductors, J.

Wiley & Sons, New York, 1967, pp. 122

24. Inoknchi, H.; and Akamatu, H.; Solid States Phys. 12, 108, 1961

25. Meier, H.; "Organic Semiconductors: Dark and Photoconductivity of Organic Solid", Verlag Chemie; Weinheim; FRG, 1974

26. Bradley, R.S.; Grace, J.D.; and Munro,D.C. Trans, Faraday Soc. 58 776, 1962

27. Kanda, S.; Kawaguchi, S.; J. Chem. Phys. 34, 1070, 1961

28. Rutkowsky, J.; Drost, H.; and Timm,U.; Exp. Tech. Phys. 16, 342, 1968

29. Felding,P.E.; Gutmann, F.; J. Chem. Phys. 26, 411, 1957

30. Okamoto, Y.; Brenner, W.; Organic Semiconductors, Reinhold Publ. Corp., New York, 1964

31. Inokuchi, H.; and Akamatu,H.; Solid State Phys. 12, 93, 1961

32. Kearn, D.R.; and Calvin, M.; J. Chem. Phys. 34, 2022, 1961

33. Fabish, T.J.; Saltsburg, H.M.;and Hair, M.L.; J. Appl. Phys. Vol. 47, No. 3, 930-939, March 1976

34. Fabish, T.J.; Saltsburg, H.M.;and Hair, M.L.; J. Appl. Phys. Vol. 47, No. 3, 940-948, March 1976

35. Fabish, T.J.; and Duke, C.B.; J. Appl. Phys. Vol.48, No. 10, October 1977

36. Duke, C.B.; and Fabish, T.J. J. Appl. Phys. 49(1), January 1978

37. a. Weaire, D.; Phys. Rev. Letters 26,1541, 1971

b. Weaire, D.; Thorpe, M.F.; Phys. Rev.;B4, 2508, 1971

c. Physics Today 24, 17, 1971; 25, 9, 1972

38. Sze,S.M. Physics of Semiconductor Devices; John Wiley & Sons New York. london 1967

39. Eley, D.D.;"Energy gap and pre-exponential factor in dark conduction by organic semiconductoes"; J. Polymer Sci. C 17, 73-91, 1967

40. Eley, D.D; Fawgett, A.S.; and Willis, M.R.;" Semiconductivity of organic substances. Electrode injection of charge carriers into crystals of small aromatic molecules"; Trans. Farada Soc. 64, 1513-27, 1968

41. Eley, D.D; Inokuchi, H.; and Willis, M.R.; "The semiconductivity of organic substances. Part 4: Semiquinone type molecular complexes"; Discuss. Farada Soc. 28, 54-63 1959

42. Eley, D.D.; Farfitt, G.D." The semiconductivity of organic substances. Part 2" Trans. Farada Soc. 51, 1529-39, 1953

43. Eley, D.D.; Parfitt, G.D.; Perry, M.J.; and Taysum, D.H.;"The semiconductivity of organic substances. Part 1" Trans. Farada Soc. 49, 78-86, 1953

44. Eley, D.D.; and Spivey, D.J.;" The semiconductivity of organic substances. Part 6" , Trans. Farada Soc. 56, 1432-42, 1960

45. Eley, D.D.; and Spivey, D.J.;" The semiconductivity of

organic substances. Part 8: Porphyrins and dipyromethenes" Trans. Farada Soc. 58, 405, 1962

46. Rose,A.; and Lampert,M.A. Phys. Rev. Vol.113, No.5, Mar.1 1959

47. rose,A.; CAL Rev.; Vol.97, No.6 ; Mar.15, 1955

48. Mott, N.F.; and Gurney, R.W.; Electronic Processes in Ionic Crystals, Oxford University Press, New York, 1940

49. Weimer, P.K. and Cope, A.D.; RCA Review 12, 314, 1951

50. Rose, A.; RCA Review 12, 362, 1951

51. Smith, R.W. and Rose, A.; Phys. Rev. 92, 857, 1953

52. Shockley, W. Prim. Phys. Rev. 90, 735, 1953; Acey, G.C. Phys. Rev. 90, 759, 1953

53. Buke, R.H. and Thomsen, S.M.; J. Chem. Phys. 23, 15, 1955

54. Simmons, J.G.; and Tam, M.C. Phys. Rev.B, Vol.7, No 8 15 Apr. 1973

55. Simmons, J.G.; and Taylor, G.W. Phys. Rev. B 5 1619, 1972

56. Simmons, J.G.; and Taylor, G.W. Phys. Rev. B 4, 502, 1971

57. Garlick, G.F. and Gibbon, A.F.; Proc. Phys. Soc. 60, 574, 1984

58. Grossweiner, L.I.; J. Appl. Phys. 24, 1306, 1953

59. Nicolas, R.H. and Woods, J. Brit. J. Appl. Phys. 15, 783, 1964

60. Haering, R.R. and Adams, E.N.; Phys. Rev. 117, 2, 1960

61. Dussel, G.A. and Bube, R.H.; Phys. Rev. 155, 764, 1967

62. Chen, R.; J. Appl. Phys. 40, 570, 1969

63. Kelly, P. and Braunlish, Phys. Rev. 131, 1587, 1970

64. Schmidlin, F.W.; Phys. Rev. B , V. 16, No. 6, 15 Sept. 1977

65. Samo , A.; Samo , M.; Sworakowski, J.; Thomas, J.M. and Williams, J.O.; Phys. Stat. Sol.(a) 37, 271, 1976

66. Samo , A.; Samo , M.; Sworakowski, J.; Phys. Stat. Sol.(a) 36, 735, 1976

67. Kokado, H. and Schneider, W.G.; J. chem. Phys. 40, 2937, 1964

68. Thomas, J.M.; williams, J.D. and Cox, G.A.; Trans. Faraday Soc. 64, 2496, 1968

69. Scher, H. and Lax, M.; Phys. Rev. B, V.7, No.10. 4491-4502, 4502-4519, 15 May 1973

70. Spear, W.E.; J. Non-Crystalline Solids 1, 197, 1969

71. Fritzsche, H.; J. Non-Crystalline Solids 6, 49, 1971

72. Bube, R.H., Ed.;" Electronic Properties of Materials"; McGraw-Hill, New York, 1971

73. Duke, C.B.; and Fabish, T.J.; Phys. Rev. Lett.; 37, 1075, 1976

74. Duke, C.B.; Fabish, T.J.; and Paton, A.; Chem. Phys. Lett., 49, 133, 1977

75. Duke, C.B.; Paton, A.; Salaneck, W.R.; Thomas, H.R.; Plummer,E.W.; Heeger, A.J. and MacDiarmid, A.G.; Chem. Phys. Lett., 59, 146, 1978

76. Duke, C.D.; Salaneck, W.R.; Fabish, T.J.; Ritsko, J.J.; Thomas, H.R. and Paton, A.; Phys. Rev. 13, 18, 5717, 1978

77. Fabish, T.J.; CRC Crit. Rev. Solid State Mater. Sci., Dec. 1979

78. Duke, C.B. ; Mol. Cryst. Liq. Cryst., 50, 63, 1979

79. Seanor, D. A. in Electrical properties of polymers; Seanor, D. A. Ed; Academic Press; New York, London 1982; P34.

80. Andrew Nevin, W.; Chamberlain, G.A. J. Chem Soc.,Faraday Trans.2, 1989, 85(11) P 1729-1745; 1747-1764

81. Chamberlain, G.A.; Solar Cells, 8, 47, 1983

82. Chamberlain, G.A.; Cooney, P.J. and Dennison, S. Nature(London), 289, 49, 1981

83. Chamberlain, G.A. and Malpas, R.E.; Faraday Discuss, Chem. Soc. 70, 299, 1980

84. Chamberlain, G.A. and Cooney, P.J.; Chem. Phys. Lett., 66, 88, 1979

85. Petruzzella, N.; Takeda, S. and Nelson, R.C. J. Chem. Physics 47.4247 1967

86. Ashcroft, N.; Mermin, N.D. Solid state Physics; Holt,Rinehart and Winston, 1976

87. Blakemore, J.S.; Semiconductor Statistics, Pergamon Press, New York, 1962

88. Moll, J.L.; Physics of Semiconductors, McGraw-Hill Book Co., New York, 1964

89. Bube, R.H.; Photoconductivity of Solids, John Wiley and Sons, New York, 1960

90. Sadasiv, G.; Photoconductivity, Ed. Biberman, L.M., Photoelectronic Imaging Devices; Plenum Press, Newyork -London, 1971